Histone Demethylase JMJD1A Regulates Metabolism in Adipose Tissue

(ヒストン脱メチル化酵素 JMJD1A による代謝制御機構の解明)

藤原　庸右

博士学位論文

Histone Demethylase JMJD1A Regulates Metabolism in Adipose Tissue

ヒストン脱メチル化酵素 JMJD1A による代謝制御機構の解明

Yosuke Fujiwara

藤原　庸右

Table of contents

Abstract

The adaptation to chronic environmental stress often promotes a lasting adaptive phenotype, which is associated with epigenetic modifications that provide “cellular memory”. A fundamental question, which is not well understood so far is how specific environmental stressors influence specific “cellular memory” presumably via specific epigenetic programs. In the current study, using “Beige-ing of subcutaneous white adipose tissue as a model of the adaptive response against chronic cold stress, we show the mechanism for β-adrenergic signal triggered adaptation to chronic cold exposure is “memorized” in the form of epigenetic re-writing through histone demethylation by the H3K9me2 demethylase JMJD1A. This occurs via signal sensing PKA-phosphorylation of JMJD1A that nucleates the formation of a protein complex containing PPARγ, PGC-1α and PRDM16 at PPARγ binding sites in chromatin (step 1) followed by demethylation of neighboring histones at H3K9me2 (step 2). This two-step mechanism ensures a stable gene expression pattern of genes required for sustained activation of thermogenesis required in response to chronic cold exposure.

Introduction

By acute cold stress, JMJD1A, an H3K9 demethylase, up-regulates thermogenic gene expressions through β-adrenergic signaling in brown adipose tissue (BAT). Aside BAT-driven thermogenesis, mammals also have another mechanism to cope with long-term cold stress by inducing the browning of subcutaneous white adipose tissue (scWAT). Here, we show that this occurs through a two-step process that requires both β-adrenergic dependent phosphorylation of S265 and demethylation of H3K9me2 by JMJD1A. The histone demethylation independent acute *Ucp1* induction in BAT and demethylation dependent chronic *Ucp1* expression in beige-scWAT provide complementary molecular mechanisms to ensure an ordered transition between acute and chronic adaptation to cold stress. JMJD1A mediates two major signaling pathways, namely, β-adrenergic receptor and PPAR activation, via PRDM16-PPARγ-P-JMJD1A complex for beige adipogenesis. S265-phophorylation of JMJD1A and following demethylation of H3K9me2 might prove to be a novel molecular target for the treatment of metabolic disorders via promoting beige adipogenesis. Cold stress is a major threat for warm-blooded animals and therefore adaptive thermogenesis to combat cold stress is crucial for survival. Brown adipose tissue (BAT) specifically plays a critical and rapid role in thermogenesis by dissipating chemical energy to produce heat (i.e. nonshivering thermogenesis). Recent studies indicate that mammals have an additional type of thermogenic adipocyte termed beige (or brite) that resides in predominantly subcutaneous white adipose depots that provides a more sustained thermogenic response to chronic cold stress (ref [1] also reviewed in [2, 3]). The signature thermogenic protein in both brown and beige adipocytes is uncoupling protein-1 (UCP1), which stimulates thermogenesis by uncoupling cellular respiration from mitochondrial ATP synthesis [4, 5], however, BAT and beige cells display different temporal patterns of *Ucp1* expression that likely contribute to their different roles in the comprehensive thermogenic response [2]. In BAT, *Ucp1* is expressed at constitutively high basal levels before cold stress [6] whereas in scWAT, *Ucp1* expression is normally very low but it is induced

to a very high level in response to chronic environmental cold stress (and also in response to exposure to agonists for β-adrenergic receptor or PPARγ [1, 7]). The actions of *Ucp1* dependent thermogenesis in BAT and scWAT beige cells likely provide a coordinated adaptive response to efficiently link the acute and chronic phases of cold stress-dependent uncoupled respiration.

JMJD1A (also known as JHDM2A or KDM3A) is an histone H3 lysine 9 (H3K9) di- and mono-methyl (me2/1) demethylase with broad functional roles in stem cell renewal [8], spermatogenesis [9], sex determination [10], and cancer [11, 12]. It is also a crucial regulator of normal body weight control and acute thermogenesis in BAT [13, 14, 15]. A previous study reported that β-adrenergic receptor (BAR) dependent induction of *Ucp1* in brown adipocytes under acute cold exposure required the demethylase JMJD1A [14]. They proposed the activation of *Ucp1* required JMJD1A demethylase activity because BAR stimulation in a cultured line of brown adipocytes resulted in a decrease of H3K9me2 on the *Ucp1* gene enhancer, and this effect was lost when JMJD1A levels were reduced by a knockdown approach. This result was unexpected because *Ucp1* is constitutively expressed at a high basal level in BAT before cold stress indicating the *Ucp1* locus already has features of euchromatin. Therefore, a high level of the repressive H3K9me2 histone mark at the *Ucp1* locus in BAT was not expected. In addition, alterations in histone methylation are usually associated with long-term lasting memory transitions such as terminal cell differentiation (reviewed in [16, 17, 18]). Therefore, the previous study was potentially complicated and more detailed studies were necessary to address the functional role of JMJD1A in thermogenic regulation.

In a more recent report we uncovered a novel role for JMJD1A in acute induction of *Ucp1* and *Adrb1* gene expression in BAT in response to BAR signaling. We showed that BAR signaling resulted in PKA dependent phosphorylation and chromatin recruitment of JMJD1A to PPARγ target sites in *Ucp1* and *Adrb1* locus regulatory regions [13]. Importantly, the induction was not accompanied by a decrease in H3K9me2 of the *Ucp1* enhancer (Supplementary Fig. 3b in ref [13]), nor did it depend on JMJD1A

demethylase activity (Fig. 3d in ref [13]). Instead, we showed that after phosphorylation, JMJD1A facilitated long-range chromatin interactions to facilitate BAR signal dependent gene expression (i.e. through dynamic higher ordered chromatin structure) [13]. This phosphorylation dependent, but H3K9me2 demethylation independent BAR induction mechanism functions on top of other chromatin regulatory events (e.g. histone acetylation [13]) that allow constitutive high expression of *Ucp1* in BAT. Acute cold stress triggers phosphorylation cascades leading to immediate heat production in BAT, while chronic cold stress promotes a lasting adaptive thermogenic phenotype through activation of the beige cell program in scWAT that is thought to be associated with alterations in methylation of DNA and/or histones [19]. However, how chronic cold stress and downstream β-adrenergic signaling is sensed by epigenetic enzymes, and how they provide a sustained thermogenic response was not understood. Therefore, we investigated a putative role for BAR activated JMJD1A in beige-ing of scWAT.

Material & Methods

Mice

Jmjd1a-null (-/-) mice (C57BL/6J background) were described previously [15].

Generation of *Jmjd1a*-S265A$^{KI/KI}$ mice. A targeting plasmid was constructed by using genomic DNA fragments derived from RENKA mice. A neomycin cassette flanked by two loxP sites in intron 8 as 3' homologous arm and S265A point mutation site (TCT (Ser) → GCA (Ala)) in exon 5-8 as 5' homologous arm was introduced into the *Jmjd1a* locus of ES cells (derived from the RENKA strain). Electroporation, selection, and screening were performed with standard gene-targeting techniques. Chimeric males were generated by using the morula aggregation technique and mated to CAG-Cre female mice to obtain *Jmjd1a*-S265A$^{+/KI}$ mice removed the neomycin-resistant gene. After achieving germline transmission, *Jmjd1a*-S265A$^{+/KI}$ mice were back-crossed with C57BL/6N mice, and the C57BL/6N background *Jmjd1a*-S265A$^{+/KI}$ mice were mated to obtain *Jmjd1a*-S265A$^{KI/KI}$ mice. Genotyping of mice used in this study was performed by PCR of tail DNA followed by direct sequencing or PstI digestion as shown in Figure 5a; S265A mutation was decided when a 700 bp PCR product produced by a pair of oligonucleotides (5'-gcttggacccatctactcagtg-3' and 5'-caagatctggaacttgtaaca-3') was digested by PstI and divided into two DNA fragments (200 bp and 500 bp).

Animal experiments

All animal studies were approved by the Animal Care and Use Committee of The University of Tokyo. Mice were maintained under a 12 hr light/12 hr dark cycle (08:00-20:00) at constant temperature (23ºC) with free access to food and water. Animals were fed a normal chow diet (CE-2, CLEA Japan Inc.) or high-fat diet consisting of 58.0% fat, 15.0% protein, and 27.0% carbohydrate from calories

from the age of 4 weeks as indicated [20, 21] .

For chronic cold exposure experiments, animals were single-caged and exposed to 4ºC for 1 week unless otherwise stated. At the conclusion of experiments, tissues were harvested and snap frozen in liquid nitrogen for RNA and protein analysis or fixed in 10% formalin for histology.

To analyze the BAT thermogenic function *in vivo*, we examined whole animal oxygen consumption following intraperitoneal injection of norepinephrine (NE) (1 mg per kg BW) for 1 hr, the standard activator of BAT-mediated thermogenesis. On the day of the experiment, mice were first placed in metabolic chambers at 30°C, sedated with 2,2,2-tribromoethanol (36 mg per kg BW, T48402; Sigma) followed 15 min later by NE injected. Energy expenditure was measured using indirect calorimetry (MK-5000RQ; Muromachi) [13]. The chamber volume was 720 ml, airflow to the chamber was 400 ml min^{-1} for 30°C-acclimated mice and 800 ml min^{-1} for 4°C-acclimated mice. Samples were taken every 3 min and a standard gas reference was taken every 30 min.

Details of the age and sex of mice used are shown in the **Table 1**.

Body temperature. Core body temperature was monitored using a rectal thermometer (Bio research center; BDT-100 C). Mice were acclimated to thermoneutrality (30°C) for 4 week prior to the experiments of acute cold exposure. The body temperature was measured at 8-9 weeks of age in control and *Jmjd1a*-S265A$^{KI/KI}$ mice at 10 a.m.

Plasma parameters. Plasma glucose concentrations were measured by Glucose C2-test (Wako). Plasma insulin level was determined by ELISA using an insulin immunoassay kit (Shibayagi), according to the manufacturer's instructions.

Glucose and insulin tolerance tests. For glucose tolerance test (GTT), mice were fasted for overnight

and then given an intraperitoneal injection of glucose (2 g per kg body weight) [15]. For insulin tolerance test (ITT), non-fasted mice were injected intra-peritoneally 4 hr after beginning of light cycle with 0.4 U per kg body weight of human insulin (Humalin® R, Eli Lilly & Co., Japan). Blood samples for glucose and insulin measurements were obtained from the tail vein at the indicated times.

Antibodies.

Mouse monoclonal antibodies immunoglobulin G -F1411 (IgG-F1411) and IgG-F1430 against mouse PRDM16 were produced by immunizing mice with affinity-purified recombinant full-length mouse PRDM16 protein. Mouse monoclonal antibody IgG-F0618 against mouse JMJD1A (a.a. 843–893) was produced by immunizing mice with gp64 fusion protein expressing baculovirus [13]. Mouse monoclonal antibodies IgG-F1628 against hJMJD1A were produced by immunizing mice with affinity-purified recombinant full length hJMJD1A protein [13]. A rabbit polyclonal phospho-specific antibody against JMJD1A-S265 was produced with a synthetic phosphopeptide corresponding to residues surrounding Ser265 JMJD1A (Ac-C-KRKS(pS)ENNGS-amide) [13]. A list of other antibodies used in this article is shown in the in the **Table 2**.

Cell culture.

Primary adipocyte cultures from scWAT and BAT. Stromal vascular fraction (SVF) from inguinal subcutaneous white adipose tissue (WAT) was obtained from 3- to 6-week-old mice as described [7,22]. Briefly, scWATs were first washed in PBS before being subjected to enzymatic digestion with 1.5 mg ml^{-1} collagenase D (Roche) and 2.4 U ml^{-1} dispase II (Roche) for 40 min at 37 °C to obtain a single-cell suspension. After digestion, the centrifuged cell pellet, termed SVF, was resuspended in the complete medium (DMEM/F12 (Sigma) containing 1.2 g l^{-1} $NaHCO_3$ and 10% FBS) before serial filtration through a 100 □m nylon cell strainer (BD Falcon). To remove red blood cells, immune cells

and other contaminants, SVFs were then plated in collagen coated plates and, 1-2 hr later, medium was aspirated, wash with PBS twice, and added fresh medium. Primary brown adipocytes form SVFs were fractionated and cultured according to published methods [7, 22]. SVF from interscapular brown adipose tissue (BAT) were isolated from 1-3 day-old mice.

Adipocyte differentiation. Induction for beige adipocyte from inguinal scWAT was performed as described previously [7, 22] with modification as follows. Briefly, primary preadipocytes cultured to ~100% confluence in complete medium were induced for differentiation with induction medium (i.e. complete medium containing 0.125 mM indomethacin, 5 μM dexamethasone, 0.5 mM 3-isobutyl-1-methylxanthine, 0.5 μM rosiglitazone (ROS), 5 μg ml^{-1} insulin, and 1 nM T3) (Day 0). After 2 days, cells were incubated in the maintenance medium with 0.5 μM rosiglitazone (i.e. complete medium containing only insulin, T3 and rosiglitazone) for another 5 days. On day 7, unless otherwise stated, medium was switched to maintenance medium without rosiglitazone (i.e. complete medium containing only insulin and T3) and cultured another 1 day before the assay (Day8).

Immortalized preadipocytes (im-scWATs) derived from inguinal scWAT that were established by infecting isolated stromal vascular fractions (SVFs) of inguinal WAT with retrovirus expressing large T antigen pBabe SV40 Large T antigen from Addgene (no. 13970) [7 22]. For beige adipocyte induction im-scWAT preadipocytes were cultured in Dulbecco's modified Eagle's medium (DMEM) supplemented with 10% fetal bovine serum at 37 °C in 5% CO_2 to confluent (Day 0), and then treated with the culture medium containing 0.125 mM indomethacin, 5 μM dexamethasone, 0.5 mM 3-isobutyl-1-methylxanthine, 0.5 μM rosiglitazone, 5 μg ml^{-1} insulin, and 1 nM T3 for 48 hr (Day 2), followed by treatment with only insulin, T3 and rosiglitazone for another 6 days with medium replacement every 2 days (Day 8) [7, 22].

For brown adipocytes induction from SVF of BATs, cells were induced for differentiation with DMEM/HAMF12 medium containing 5 μg ml^{-1} insulin, 1 nM T3, 0.125 mM indomethacin, 5 μM

dexamethasone, and 0.5 mM 3-isobutyl-1-methylxanthine for 2 days. From day 2, cells were cultured only in the presence of insulin and T3.

β-adrenergic receptor activation and antagonist treatment. To activate β-adrenergic receptor (BAR) in tissue culture experiment, norepinephrine (10 μM for 1-2 hr) or non-selective BAR agonist isoproterenol (ISO, 1 μM) was added to culture medium. To block BAR activation, 100 nM of propranolol (Pro) was added as described under the legends for figures. In mice study, 1 mg per kg body weight (BW) of NE was intraperitoneally injected as described under Animal Experiments.

Oil red O staining. Cells at the specified stage of differentiation were rinsed with PBS (PBS) and fixed with 3.7% formaldehyde in H_2O for 10 min. After 2 washes in PBS and 1 wash with 60% isopropanol for 1 min, cells were stained for 15 min in freshly diluted ORO solution (0.18% (wt/vol) ORO in 60% isopropanol). The stain was then removed, and cells were washed twice with PBS and photographed.

Retroviral vectors and infection. To construct a retroviral vector for JMJD1A (pMXs-hJMJD1A-V5-IRES/Zeo), we subcloned DNA sequence encoding human JMJD1A open reading frame (ORF) into an expression vector pMX (a kind gift from Dr. Toshio Kitamura, The University of Tokyo) driven by LTR promoter, in which the original puromycin-resistant sequences were replaced by Zeocin™-resistant sequences [13]. Mutant versions of hJMJD1A: S265A, S265D, or S265D-H1120Y were generated by PCR-based site-directed mutagenesis. To construct retroviral vector for shRNA targeting Jmjd1a, forward primer 5'-gatctttgccgatgacctttcagataattcaagagattatctgaaaggtcatcggttttgttcc-3' and reverse primer 5'-agctggaacaaaaccgatgacctttcagataatctcttgaattatctgaaaggtcatcggcaaa-3' were annealed and subcloned into a mouse U6 promoter-driven expression vector pRetro/Puro-Super3 (a kind gift from Dr. T. Kitamura) in which puromycin resistant marker sequences were replaced by neomycin

resistant marker sequences. Retroviruses were produced by transfecting each plasmid into Platinum-E (Plat E) packaging cells (a kind gift from Dr. T. Kitamura) using GeneJuice (Novagen). To establish JMJD1A knockdown immortalized adipocytes, im-scWATs were transduced with retroviral vector expressing shRNA targeting murine *Jmjd1a* under the control of U6 promoter and were selected by G418 (1 mg ml^{-1}) for 6 days. To establish im-scWATs ectopically expressing WT or mutants JMJD1A, the resultant JMJD1A knockdown im-scWATs were infected with retrovirus expressing WT, S265A, S265D, or S265D-H1120Y and infected cell were selected by Zeocin treatment (0.1 mg ml^{-1}) for 12 days [13, 23].

Co-imunoprecipitation and immunoblot analysis. Whole-cell lysates were collected in cell lysis buffer A (50 mM HEPES-KOH, pH 7.9, 150 mM NaCl, 1.5 mM $MgCl_2$ and 1% NP-40) containing both protease inhibitors (5 μg ml^{-1} pepstatin A, 10 μg ml^{-1} leupeptin, 2.8 μg ml^{-1} aprotinin, 1 mM DTT and 0.5 mM PMSF) and phosphatase inhibitors (40 mM NaF and 1 mM Na_3VO_4). JMJD1A or PRDM16 protein was immunoprecipitated in cell lysis buffer A for 6 hr at 4 ºC using the antibodies described in the legend to figures. Co-immunoprecipitates were subjected to SDS-PAGE and immunoblots were visualized by chemiluminescence using Super Signal West Dura Extended Duration Substrate (Thermo Fisher Scientific), and luminescent images were analyzed by ImageQuant LAS 4000mini (GE Healthcare) [13,23]. For immunoblot analysis of histones, histones were acid extracted from BAT or scWAT of C57BL/6J mice using a Histone Purification Mini Kit (Active Motif) following the manufacturer's instructions as described [24].

Chromatin immunoprecipitation (ChIP) and ChIP-seq. The procedures for H3K9me2 ChIP assay using adipose tissues of mice were performed as follows. Fresh scWATs or BATs were minced, cross-linked with 0.5% (vol per vol) formaldehyde for 10 min, homogenized with Dounce type homogenizer in

ice-cold hypotonic buffer B (10 mM HEPES-KOH, pH 7.5, 1.5 mM $MgCl_2$, 10 mM KCl, 1 mM EDTA, 1 mM EGTA containing 1 mM PMSF and protease inhibitor cocktail (Nacalai Tesque)), and centrifuged at 1,000 x g for 7 min to obtain nuclear fraction. Cross-linked nuclear fractions were lysed in cell lysis buffer C (23 mM Tris-HCl, pH 8.0, 3.0 mM EDTA, 0.9% Triton X-100, 134 mM NaCl, 1 mM PMSF, and protease inhibitor cocktail (Nacalai Tesque)) containing 0.2% SDS (Fig. 1d and Fig. 2c) or 0.1% SDS (Fig. 2b and 4c), sheared to 200 bp to 300 bp by using SONIFIER 250 (Branson) (output 4, duty cycle 60%, 20 sec x 15 times), and used for immunoprecipitation. The amount of DNA content in the nuclear lysate was determined after pronase protein digestion and DNA purification. For H3K9me2-ChIP, 3 μg nuclear DNA containing nuclear lysates were immunoprecipitated for 2 hr at 4°C with 2 μg of anti-H3K9me2 antibody (IgG-6D11) [25] pre-bound to 50 μl of Dynabeads protein G (Life Technologies). The immunoprecipitated DNA was subjected to qPCR with SYBR green fluorescent dye [13, 23]. H3K9me2 ChIP using mouse scWAT, ChIP in cell lysis buffer C containing 0.1% SDS (Fig. 2b and 4c) gave higher amount of precipitated DNA compared to that in cell lysis buffer C containing 0.2% SDS (Fig. 1d).

For ChIP-seq analysis using JMJD1A antibody, precipitated DNA from original DNA size of ~2 kb was further sheared to ~200 bp by an Acoustic Solubilizer (Covaris). For ChIP-seq using PPARγ antibody, DNA sonicated to be 0.5 kb average in size was used for ChIP. Chromatin immunoprecipitated samples were used for library preparation-with KAPA Hyper Prep Kit (Nippon Genetics) according to the manufacturer's instructions [13, 23]. Deep sequencing was performed on a HiSeq2500 sequencer (Illumina) as single-end 50 base reads. All bound DNA fragments were mapped to UCSC build mm9 (NCBI Build 37) assembly of the mouse genome by a mapping program ELAND (Illumina) based on the 36 bp sequences. Signals of ChIP-seq occupancy are presented as reads per million mapped reads (RPM).

Quantitative real-time qPCR (qPCR). qPCR was carried out in 384-well plates using the ABI PRISM 7900HT sequence detection system (Applied Biosystems). All reactions were done in triplicate. All primer sequences used in this article are listed is shown in the **Tables 3 and 4**. Copy numbers of *Ucp1* mRNA in BAT and scWAT were determined by qPCR as described [24] using a plasmid containing mouse *Ucp1* open reading frame as the standard template for *Ucp1*. The data were converted to copy number per ng of total RNA.

RNA-sequencing. Total RNA of cells was isolated using ISOGEN (Nippon Gene) according to the manufacturer's protocol. RNA-sequencing (RNA-Seq) libraries were prepared by TruSeq sample purification kit (Illumina). The libraries were sequenced on HiSeq 2500 (Illumina), and the reads were aligned to mouse transcriptome (UCSC gene) and genome (mm9) references respectively using Burrows-Wheeler Aligner. After transcript coordinate was converted to genomic positions, an optimal mapping result was selected either from transcript or genome mapping by comparing the minimal edit distance to the reference. Local realignment was performed within in-house short reads aligner with smaller k-mer size (k=11). Finally, fragments per kilobase of exon per million fragment mapped (FPKM) values were calculated for each UCSC gene while considering strand-specific information. When expression alterations were analyzed, gene expression levels are presented as $\log_2$ fold change in FPKM relative to those in indicated controls.

Analysis of transcription factor-binding motifs. Transcription factor binding motif analysis was performed using TRAP, in which the algorithm ranks the known binding motifs in the descending order of the enrichment in target genomic sites [26]. The JMJD1A binding sites [13] from ChIP-seq data were extracted by SICER using the default parameter setting: window size, 200 bp; gap size, 400 bp; E-value threshold, 100. Subsequently, the PPARγ binding sites [13], and the PRDM16-binding sites [27]

from ChIP-seq data were extracted by MACS using the default parameter setting: p-value threshold, 5e-10; band width, 300 bp; shift size, 100 bp. The sites co-localized by JMJD1A, PPARγ, PRDM16, and those localized by only JMJD1A were respectively obtained by comparing the overlaps among the factor bindings. In the two datasets, after the sizes of all the binding sites were converted to 500 bp, the sites with top-300 JMJD1A binding signals were selected as the input data of TRAP. After that, the enriched binding motifs were predicted, compared with random promoters. As the reference motifs, we used those archived in JASPAR, the database of the known binding motif.

Measurements of oxygen consumption. Oxygen consumption was measured using a Seahorse XF24 extracellular flux analyzer as described previously [13]. Briefly, cultured adipocytes at day 7 of differentiation were detached with Trypsin (0.5 g l^{-1})/EDTA (0.53 mM) solution (Nacalai Tesque) and re-seeded at 5.0 x10^4 or 1.0 x10^5 cells per well for brown adipocytes and white or beige adipocytes, respectively, into XF24 V7 cell culture microplates (Seahorse Bioscience). First, basal respiration was assessed in untreated cells. Second, ATP turnover was calculated in response to 40 μg ml^{-1} oligomycin (Oligo) (Wako). Third, maximum respiratory capacity was assessed after the stimulation by 2.5 μM carbonyl cyanide 4-(trifluoromethoxy) phenylhydrazone (FCCP) (Sigma). Finally, mitochondrial respiration was blocked by adding both 1 μM rotenone (Rot) (Sigma) and 1 μM Antimycin A (Anti) (Wako) and the residual OCR was considered as non-mitochondrial respiration. Proton leak was calculated by subtracting the ATP turnover and the non-mitochondrial respiration components of basal respiration as described previously [13]. To assess the oxygen consumption of the mouse scWAT, the adipose tissues (1.5 mg) from mice housed at 30 ºC or 4 ºC for 1 week were isolated, minced, and placed into XF24 Islet Capture Microplates (Seahorse Bioscience) and the basal OCR was monitored after pre-incubation for 1 hr with the XF24 assay media.

Glycerol release. Norepinephrine (NE)-stimulated glycerol release from differentiated adipocytes from cultured differentiated adipocytes (i.e. hJMJD1A-transduced immortalized adipocytes or SVF of BAT or scWAT) was measured using a Lipolysis Assay Kit (ZenBio) as described [13]. Differentiated adipocytes on day 7 were detached with Trypsin (0.5 g l^{-1})/EDTA (0.53 mM) Solution (Nacalai Tesque) and re-seeded at 2.5 x10^5 cells and 1.5 x10^5 cells for brown and white adipocytes, respectively, into 96-well plate. On the next day (Day 8), cells were treated with NE (10 μM) for 1 hr at 37°C. The optical density of produced quinoneimine dye was measured at 540 nm.

Mitochondria quantity analyses. For quantification of mitochondrial DNA (mt-DNA) copy number, mt-DNA was isolated from cultured adipocyte by phenol/chloroform after digestion with Proteinase K (100 μg ml^{-1}) at 37°C overnight. Relative amounts of nuclear DNA and mt-DNA were determined by quantitative real-time PCR. We selected NADH dehydrogenase 1, 2 or 4 - coding gene (*Nd1*, *Nd2* or *Nd4*, respectively) and *Cyclophilin* (*Ppib*) for nuclear DNA quantification. For MitoTracker staining, cells were incubated with 100 nM Mito Tracker Green FM dyes (Molecular Probes) for 30 min at 37°C. After staining, the cells were washed with pre-warmed PBS. Immunofluorescence was captured with LEICA DMI 6000B microscope (Leica microsystems).

Immunohistochemistry. BAT and scWAT isolated from mice were placed in 10% formalin for 48 hr, stored in 70% ethanol, and subsequently paraffin embedded. Immunostaining was performed on deparaffinized 3 μm sections which were rehydrated and quenched endogenous peroxidase activity by the treatment with 3% hydrogen peroxide for 15 min. Following antigen epitope retrieval performed by autoclaving slides in Tris buffer (pH9.0), the sections were incubated overnight at room temperature with either mouse monoclonal anti-UCP1 antibody (ab10983, Abcam) at a dilution of 1:1,000. The bound anti-UCP1 was detected by rabbit anti-mouse secondary antibody followed by biotin-free

horseradish peroxidase-labeled polymers (DAKO). Bound horseradish peroxidase-labeled polymers were detected by addition of 3,3-diaminobenzidine substrate-chromogen solution and counterstained with hematoxylin.

Electron microscopy analysis. Cell pellets were fixed in 2.5% glutaraldehyde in 0.1 M phosphate buffer (pH 7.4). Post-fixation was performed in 1% osmium tetroxide (OsO_4) in 0.1 M phosphate buffer (pH 7.4). Subsequently, samples were dehydrated and embedded in epoxy resin (*Quetol-651,* Nissin EM). Ultrathin sections (100 nm) were cut by an ultramicrotome (Ultracut N, Reichert-Nissei) and collected on grid meshes. The sections were stained with 1% uranyl acetate for 10 min, followed by 1% lead citrate for 5 min, and washing with distilled water. They were examined with an electron microscope (Hitachi H-600A, Hitachi).

Statistical analysis. All data are presented as mean ± s.e.m. Student's t-test was performed for the comparison of two groups. For multiple comparisons, analysis of variance was performed followed by Tukey's post hoc comparison. $*P < 0.05$, $**P < 0.01$ and $***P < 0.005$. Significance was considered as $P < 0.05$.

Data availability. RNA-seq transcriptome data and ChIP-seq data reported in this paper is deposited to Gene Expression Omnibus in the accession number of GSE107901.

Result

H3K9me2-independent thermogenic gene inductions in BAT

H3K9me2 is a signature heterochromatin mark that facilitates chromatin condensation and gene silencing [28]. *Ucp1* is expressed at high constitutive levels in BAT but at very low level in scWAT. The high constitutive expression in BAT is consistent with the significant association of the gene enhancer and promoter activation histone marks H3K27ac and H3K4me3 with the *Ucp1* in BAT chromatin (**Fig. 1a**). This is also consistent with the selective activation of *Ucp1* following cold exposure in BAT (**Fig. 1b**) and the significantly lower levels of total (**Fig. 1c**) and *Ucp1* enhancer/promoter regions associated H3K9me2 in BAT relative to scWAT (**Fig. 1d**).

H3K9me2-dependent Beige-selective gene inductions in scWAT

In addition to the rapid activation of thermogenesis in BAT by cold stress, chronic exposure of mice to cold results in markedly induced *Ucp1* mRNA and protein in scWAT referred to as beige-ing (reviewed in [28, 3, 2]) (**Fig. 2a**). Given that *Ucp1* enhancer/promoter regions are heavily H3K9me2-methylated and silenced in scWAT before and during acute cold exposure, I reasoned that the activation of the beige-ing thermogenic program during chronic cold exposure might be associated with H3K9me2 demethylation of thermogenic gene enhancer/promoter regions. This would be consistent with prior studies demonstrating that long-term stable transcriptional changes are associated with altered chromatin methylation [28]. To examine this hypothesis, I measured enhancer/promoter regions associated H3K9me2 levels by ChIP analysis using scWAT of mice housed at RT vs 4°C for 1 week. This analysis revealed that H3K9me2 on the *Ucp1, Cidea, and Ppara* gene enhancer/promoter regions in scWAT was significantly reduced following chronic cold exposure of mice (**Fig. 2b**) while

H3K9me2 in BAT, which is very low even before cold exposure (see also **Fig. 1d**), were not significantly decreased after 1-week cold exposure (**Fig. 2c**).

Ucp1 induction in BAT and scWAT during cold exposure

To directly compare the acute activation of *Ucp1* in BAT vs. the chronic activation in scWAT, I monitored *Ucp1* over the course of a 3-week exposure of mice to 4°C. *Ucp1* mRNA in BAT was acutely activated and peaked early (6 hour), and it declined over the course of one week to half the peak value. In scWAT, *Ucp1* mRNA was barely detected during the acute phase of cold exposure, however, it significantly increased over the first week and remained at this elevated steady state level over the 3-week exposure period (**Fig. 3a**). The long-term increase in *Ucp1* expression in scWAT is also associated with a decrease in H3K9me2 at the *Ucp1* locus in scWAT during chronic cold exposure (**Fig. 1f**). These different responses raised the hypothesis that while pS265-JMJD1A acutely induces thermogenic gene expressions in BAT through a mechanism that is independent of H3K9me2 demethylation activity, in scWAT, pS265-JMJD1A might also erase H3K9me2 to provide long term activation of thermogenic genes required for adaptation to chronic cold exposure (**Fig. 3b**).

JMJD1A induces beige-selective genes

To study whether JMJD1A was involved in the beige-ing, Histological staining showed a lack of UCP1-positive beige adipocytes with multilocular lipid droplets in *Jmjd1a*-null mice after cold exposure (**Fig. 4a**). And more UCP1 protein levels increased after cold exposure in the scWAT of the *WT* while they were not increased in *Jmjd1a*-null mice (**Fig. 4b**). H3K9me2 levels on the *Ucp1*, *Cidea*, *and Ppara* gene enhancer/promoter regions was significantly higher in scWAT of cold acclimated *Jmjd1a*-null mice (**Fig. 4c**). These data suggest that JMJD1A is pivotal for the activation of beige-selective gene expression during beige-ing of inguinal scWAT.

Generation of *Jmjd1a*-S265A$^{KI/KI}$ mice

To study the physiological relevance of pS265-JMJD1A as a cold sensor in BAT and also the relationship with the H3K9me2 changes in scWAT beige-ing (**Fig. 3b**), I generated mice with a serine 265-to-alanine knock-in mutation (*Jmjd1a*-S265A$^{KI/KI}$) (**Fig.5a**). *Jmjd1a*-S265A$^{KI/KI}$ mice were born in normal Mendelian ratio and did not exhibit male infertility or male-to-female sex reversal observed in *Jmjd1a*-null mice [9, 10] (**Fig. 5b**).

Jmjd1a-S265A$^{KI/KI}$ mice reduced BAT thermogenic activity

Similar to *Jmjd1a*-null mice [13, 14], *Jmjd1a*-S265A$^{KI/KI}$ mice had reduced whole animal oxygen consumption following injection of norepinephrine (NE) in mice acclimated to 30ºC [4, 30, 31] (**Fig. 6a**) and exhibited defective adaptive thermogenesis in response to acute cold exposure (**Fig. 6b**) and a blunted NE-induced upregulation of three key genes (*Ucp1*, *Pgc1a*, and *Dio2*) involved in thermogenesis in BAT (**Fig. 6c**). Additionally, NE-stimulated oxygen consumption and glycerol release were profoundly reduced in primary brown adipocytes from *Jmjd1a*-S265A$^{KI/KI}$ mice as well (**Fig. 6d)**. In adulthood, like *Jmjd1a*-null mice, *Jmjd1a*-S265A$^{KI/KI}$ mice also had features of altered BAT including larger depot size and increased fat accumulation (**Fig. 6e**).

S265 phosphorylation of JMJD1A induces beige-selective genes

To study whether the pS265-JMJD1A was involved in the induction of beige-selective genes, I quantified the expression of thermogenic genes in scWAT of *WT* and *Jmjd1a*-S265A$^{KI/KI}$ mice housed at 30°C or following cold temperature (4°C) for 1 week. 4°C treatment induced the expression of the core set of thermogenic genes in scWAT including *Ucp1*, *Cidea*, *Pgc1a*, *Cox8b*, *Elovl3*, and *Dio2* in *WT* mice (**Fig. 7a**) but this response was severely attenuated in the scWAT of *Jmjd1a*-S265A$^{KI/KI}$ mice.

By contrast, expression of general adipogenic genes (*Pparg* and *Adipoq*) did not differ significantly between *WT* and *Jmjd1a*-S265A$^{KI/KI}$ mice. Consistent with the mRNA levels, f (**Fig. 7b**). Histological staining showed a lack of UCP1-positive beige adipocytes with multilocular lipid droplets in *Jmjd1a*-S265A$^{KI/KI}$ mice after cold exposure (**Fig. 7c**). Basal whole-body oxygen consumption rate (OCR) before NE injection was significantly higher in the 4°C-acclimated *WT* mice (55 ml h^{-1}; **Fig. 7d**) than in the 30°C-acclimated *WT* mice (40 ml h^{-1}; **Fig. 6a**). However, OCR response was 20-25% lower in *Jmjd1a*-S265A$^{KI/KI}$ mice relative to *WT* (**Fig. 7e**). This suggests that S265-phosphorylation of JMJD1A is important in the beige-ing as it is in the acute thermogenic response in BAT. Additionally, the abundant clusters of UCP1-positive adipocytes with multilocular lipid droplets and UCP1 that develop in scWAT from inguinal fat pads of *WT* mice following chronic cold exposure were significantly reduced in both *Jmjd1a*-S265A$^{KI/KI}$.

pS265-JMJD1A cell autonomously induces beige-selective genes

To evaluate whether the effect of phospho-JMJD1A on the induction of beige-selective genes in scWAT depot is cell-autonomous, I isolated primary SVFs from scWAT and beige adipocyte differentiation was induced using rosiglitazone (ROS) (hereafter I call them scWAT culture) as previously reported [7, 22]. NE induced S265-phosphorylation of JMJD1A in scWAT culture from *WT* (WT scWAT culture) but not *Jmjd1a*-S265A$^{KI/KI}$ mice (S265A knock-in scWAT culture), as shown by immunoblot analysis with a pS265-JMJD1A specific antibody (**Fig. 8a**). Both cultures differentiated with equivalent efficiency into mature lipid droplet-containing adipocytes (**Fig. 8b**, inset), however, as in scWAT of *Jmjd1a*-S265A$^{KI/KI}$ mice, S265A knock-in scWAT cultures had an impaired response to NE because expression of *Ucp1* (both mRNA and protein) along with RNAs encoding other beige selective genes (e.g. *Cidea*, *Pgc1a*, *Prdm16*, *Irf4*, *Ppara*, *Cox8b*, *Cpt1b*) were all reduced (**Fig. 8b**,**c**). Consistent with the reduced thermogenic response, levels for *Pgc1a* (mRNA and protein) and

mitochondrial specific transcripts (*Nd1*, *2* and *4*, *Cytb*, *Cox1-3*, *Atp6* and *8*) and proteins of mitochondrial oxidative phosphorylation (**Fig. 8d**) were all markedly reduced in the scWAT from *Jmjd1a*-S265A$^{KI/KI}$ mice. Staining with MitoTracker Green, a marker of mitochondrial content (**Fig. 8e**), and mitochondrial DNA content by qPCR were also significantly lower in *Jmjd1a*-S265A$^{KI/KI}$ scWAT relative to *WT* controls (**Fig. 8f**). Additionally, in electron micrographs, scWAT from *WT* were packed with mitochondria containing well-ordered cristae, whereas S265A knock-in adipocytes had a paucity of mitochondria (**Fig. 8g**). *Jmjd1a*-S265A$^{KI/KI}$ scWAT also had reduced basal-, maximal-, and uncoupling- oxygen consumption rates (OCRs) and lower NE-stimulated OCR measured by flux analyzer (**Fig.8h)** and lower NE-stimulated glycerol release (**Fig. 8i**). These data show that pS265-JMJD1A contributes to beige adipocyte formation in a cell autonomous manner

Establishment of S265A-JMJD1A immortalized preadipocyte

To further investigate the molecular mechanisms of pS265-JMJD1A on the induction of beige-selective genes, I constructed WT or mutant versions of human JMJD1A (hJMJD1A) into immortalized mouse preadipocytes [7, 22] where endogenous JMJD1A was pre-knocked-down by short-hairpin RNA (shRNA) (**Fig. 9a**). shRNA efficiently depleted endogenous JMJD1A without affecting lipid accumulation (**Fig. 9b**). Retroviruses expressing either the wild type human JMJD1A or the S265A proteins were introduced and I showed the levels of ectopic hJMJD1A expression were comparable to native mouse JMJD1A (**Fig. 9c**). The S265A virus did not affect lipid accumulation although but similar to the studies from scWAT from the *Jmjd1a*-S265A$^{KI/KI}$ mice above, the mutation did impair OCR (NE-stimulated, maximal and uncoupling), NE-stimulated glycerol release, mitochondrial content, and resulted in reduced expression of *Ucp1* mRNA and protein along with lower levels encoding, other beige-selective, and mitochondrial specific mRNAs (**Fig. 9d-j**)

Phosphomimetic S265D-JMJD1A induces beige-selective genes

I also made a retrovirus expressing an S265-phospho-mimetic JMJD1A (S265D$^{-hJMJD1A}$), in which the negatively-charged aspartyl residue mimics a negatively charged phosphate group. In contrast to the S265A mutation, when the S265D virus was introduced into the JMJD1A depleted adipocytes it resulted in dramatically elevated constitutive expression of a distinct set of beige selective genes (**Fig. 10a**). UCP1 and PGC1α protein levels were also increased (**Fig. 10b**). By contrast, expression of general adipogenic genes did not differ significantly between WT and S265D^{-}transduced cultures (**Fig 10a**). Consistent with the increased expression of *Pgc1a*, *Irf4* and *Tfam*, which are involved in mitochondrial biogenesis and function [32], S265D transduction resulted in an increased in the constitutive levels of mitochondrial DNA (**Fig. 10c**) and the relative amounts of proteins of the mitochondrial oxidative phosphorylation complexes (**Fig. 10b**). Taken together, these loss and gain of function data demonstrate that pS265-JMJD1A is essential for inducing the differentiation of beige adipocytes (mediated by TZDs) under chronic β-adrenergic signaling.

TZD-induced beige adipogenesis is mediated by p-JMJD1A

Chronic activation of PPARγ by TZDs such as rosiglitazone (ROS) and BAR activation both stimulate beige-ing in mammals (reviewed in [3, 28]). However, whether or not BAR activation is required for beige fat cell development by TZDs is not clearly understood. I previously showed that JMJD1A integrates β-adrenergic-cAMP signaling with the PPARγ gene activation program through a mechanism where pS265-JMJD1A performs a scaffolding role to activate key PPARγ target genes required for thermogenesis in BAT [13]. Because the fetal bovine serum used for cell culture contains non-negligible levels of catecholamines [13], I included the BAR blocker propranolol (Pro) during differentiation. Regardless of Pro treatment, preadipocytes differentiated into adipocytes with similar

lipid accumulation (**Fig. 11a**). Pro reduced β-adrenergic signaling because Pro blunted phosphorylation of JMJD1A on S265 (**Fig. 11b, compare lanes 2 and 3**) and Pro also markedly reduced the expression of beige-selective genes (**Fig. 11c**) and protein levels of UCP1 and mitochondrial oxidative phosphorylation complex subunits (**Fig. 11d**) along with reduced OCR (**Fig. 11e**). Furthermore, expression of beige-selective genes was markedly reduced in S265A$^{\text{-hJMJD1A}}$-transduced cultures while similar levels of general adipogenic genes were expressed in both WT$^{\text{-}}$ and S265A$^{\text{-hJMJD1A}}$-transduced cultures regardless of Pro treatment (**Fig. 11c**). These data show that chronic β-adrenergic stimulation is essential for TZD-induced beige-selective activation via the downstream pS265-JMJD1A.

PRDM16 shares binding sites on beige-selective genes with JMJD1A

PRDM16 plays a central role in BAT/Beige adipogenesis through interacting with protein complexes containing transcription (co-) factors (e.g. PPARγ, C/EBPβ, PGC1α) and an epigenetic enzyme EHMT1 (reviewed in [28, 2, 3]). EHMT1 epigenetically silences gene expression through mono- and di-methylation of H3K9 of chromatin associated with targets genes during brown adipogenesis, however, how PRDM16 activates silenced genes involved in thermogenesis in scWAT is not well understood. The genome-wide DNA binding analysis of JMJD1A and PRDM16 in brown adipocytes using ChIP-seq data reported by us and others [13, 33] showed that approximately 48% of PRDM16 binding sites overlapped with JMJD1A binding sites following β-adrenergic stimulation (**Fig. 12a**) and sites of overlap include several beige-selective genes (**Fig. 12b)**. Because PRDM16 associates with several proteins including PPARγ and PGC1α (reviewed in [3]) and pS265-JMJD1A forms a protein complex with PPARγ [13], I hypothesized that pS265-JMJD1A may interact with PRDM16 together with PPARγ and PGC1α.

pS265-JMJD1A-PPARγ-PGC1α-PRDM16 protein complex

A retrovirus expressing JMJD1A tagged with a V5-peptide was transduced into the immortalized JMJD1A knockdown adipocytes used above. I then immunoprecipitated tagged JMJD1A in WT-^{hJMJD1A}-transduced adipocytes after beige conversion and examined JMJD1A and putative proteins through co-immunoprecipitation with antibodies against PRDM16, PPARγ, and PGC1α. The result showed that JMJD1A co-immunoprecipitated PRDM16 together with PPARγ and PGC1α in the absence of Pro (**Fig. 13a, compare lanes 1 and 2**) and the levels of the signature beige proteins (i.e. PRDM16, PGC1α, and PPARγ) in the co-immunoprecipitates were greatly reduced when Pro was included in the culture medium (**Fig. 13a, compare lanes 2 and 4**). Consistent with previous reports [33, 34], PPARγ and PGC1α were co-immunoprecipitated with native PRDM16 in WT-^{hJMJD1A}-transduced adipocytes, however, not in S265A-^{hJMJD1A}-transduced adipocytes (**Fig. 13b**). There was also little evidence of interaction between the phosphorylation defective S265A-JMJD1A and PPARγ, PGC1α or PRDM16 (**Fig. 13c**). In a reciprocal manner, much stronger signals for the signature beige proteins were detected by immunoblot analysis of immunoprecipitates of V5-tagged phospho-mimetic S265D-^{hJMJD1A}-transduced adipocytes compared to those of WT-^{hJMJD1A} adipocytes (**Fig. 13d**). The association of pS265-JMJD1A and the signature beige proteins were also confirmed in primary adipocytes differentiated from SVF of *WT* and S265A$^{KI/KI}$ scWATs (**Fig. 13e**). Collectively, these results demonstrate that persistent β-adrenergic signaling mediates the formation of a multi-protein complex containing JMJD1A-PPARγ-PGC1α-PRDM16 and that phosphorylation of S265 in JMJD1A nucleates formation of the entire complex which is essential for beige-selective gene induction in scWAT (**Fig. 13f**). A common DNA biding motif in ChIP-seq peaks for all three JMJD1A, PRDM16, and PPARγ following BAR activation includes the binding motif for EBF, a key factor for browning adipocyte identity [13, 35] (**Fig. 13g**). These data also suggest that beige-selective gene inducing effects by PPARγ and PRDM16 are, at least in part, mediated by JMJD1A. Additionally, because H3K9me2

levels are constitutively high in scWAT and decline during beige conversion I hypothesized that pS265-JMJD1A-PPARγ complex might contribute to beige cell function through erasing nucleosomal H3K9me2 of beige-selective genes to convert them to a euchromatin-like state.

Demethylation by JMJD1A is pivotal for beige adipogenesis

The decrease in H3K9me2 that occurs upon recruitment of JMJD1A in scWAT suggests the catalytic activity of JMJD1A might be directly required for the demethylation associated with induction of beige-selective gene expression in scWAT. To directly analyze this, I transduced WT, S265D, or the double S265D-H1120Y mutant of JMJD1A into im-scWAT where endogenous JMJD1A was knocked down (**Fig. 14a**). The H1120Y substitution changes the catalytic histidine from the carboxyl terminal demethylase domain into a tyrosine rendering the protein catalytically dead [13]. As shown earlier, the -selective genes by facilitating the protein complex with PGC1α-PPARγ-PRDM16 (**Fig. 10a** and **Fig. 13d**), Therefore, S265D-H1120Y double mutant is an ideal tool to examine the necessity of catalytic activity of JMJD1A for the induction of beige-selective genes. As shown in **Figure 14b**, transduction of S265D$^{-hJMJD1A}$ robustly induced basal, maximal, and uncoupled respiration, by contrast, transduction with the double mutant S265D-H1120Y severely abrogated the S265D-induced respiration in beige adipocytes. These data indicate that demethylation activity of JMJD1A is absolutely required for promoting thermogenic function in the induction of beige-selective genes.

To comprehensively elucidate beige-selective genes that are dependent on both JMJD1A S265-phosphorylation and demethylation activity, I compared RNA-seq transcriptome data of WT^{-}, S265D^{-}, and S265D-H1120Y$^{-hJMJD1A}$ -transduced adipocytes. As shown in **Figure 14c**, of 126 genes that are both beige-selective and reduced in the S265A mutant cells, 47 of these genes were upregulated in S265D$^{-hJMJD1A}$-transduced cultures. The expression of 34 genes of these 47 genes including *Ucp1*, *Cidea*, *Cpt1b*, *Ppara*, *etc.* were reduced by at least half when the catalytically dead double mutant

S265D-H1120Y$^{-hJMJD1A}$ was transduced relative to the S265D constitutively active JMJD1A (FPKM score; SDHY/SD < 0.5) (**Fig. 14c**). These 34 genes are considered to mediate cellular memory because their expressions are highly dependent on demethylation activity of JMJD1A. The expression of additional 13 genes including *Otop1*, *Elov3*, and *Prdm16* were also reduced but not as much as *Ucp1* and *Cidea* (**Fig. 14c**). The expression differences for some of the key genes was confirmed by qPCR (**Fig. 14d**). Collectively, these results demonstrate that persistent cold exposure or β-adrenergic agonist stimulation induces beige adipogenesis via two steps: β-adrenergic signal sensing followed by H3K9me2 demethylation.

Insulin resistance phenotype of *Jmjd1a*-S265A$^{KI/KI}$ mice

Beige adipocyte activity affects systemic metabolism and significantly contributes to whole body insulin sensitivity [6, 36, 37]. Therefore, I investigated whether abrogation of beige fat recruitment in *Jmjd1a*-S265A$^{KI/KI}$ mice also results in global metabolic dysfunction. For these studies, *WT* and *Jmjd1a*-S265A$^{KI/KI}$ mice were fed on a high fat diet (HFD) and housed at 30°C for 4 weeks, and then switched to 4°C for an additional 4 weeks on the HFD. Body weight gain and glucose tolerance were similar in *WT* and *Jmjd1a*-S265A$^{KI/KI}$ mice (**Fig. 15a**). However, insulin levels in the *Jmjd1a*-S265A$^{KI/KI}$ mice were higher than *WT* mice during the glucose tolerance test (GTT) despite their comparable glucose levels (**Fig. 15b**). Consistently, insulin tolerance test (ITT) demonstrated that insulin mediated suppression of plasma glucose was significantly impaired in *Jmjd1a*-S265A$^{KI/KI}$ mice (**Fig. 15c**). Glucose and insulin levels during the GTT and ITT did not differ between *WT* and *Jmjd1a*-S265A$^{KI/KI}$ mice before cold acclimation (**Fig. 15d**) indicating that HFD fed *Jmjd1a*-S265A$^{KI/KI}$ mice have impaired insulin signaling only when the animals encounter the additional stress of cold exposure. This was further confirmed by insulin signaling studies, which revealed that loss of S265 phosphorylation impaired insulin action, as quantified by the phosphorylation of S473 on AKT in

scWAT, BAT, and soleus muscle (**Fig. 15e**). These systemic differences are likely to be due at least in part to the reduced beige recruitment and activity in the HFD fed cold acclimated *Jmjd1a*-S265A$^{KI/KI}$ mice because there was no significant difference in insulin action at RT (**Fig. 15f**).

Discussion

Beige and brown adipocytes have thermogenic activity, but they are postulated to have complementary functions in the maintenance of energy balance and thermogenesis [2]. BAT mediates acute and robust thermogenic activity while scWAT derived beige adipocytes contribute to an adaptive response against chronic cold exposure. It is likely that the combined action of *Ucp1* dependent thermogenesis in BAT and beige scWAT is physiologically important to ensure acute and chronic BAR dependent uncoupled respiration for protection from cold environmental challenges where BAR dependent uncoupling is needed (**Fig. 16**, top). We show that these complementary mechanisms for thermogenic gene induction in acute and chronic cold stress occur via overlapping but distinct mechanisms (**Fig. 16**, bottom). The acute response in BAT requires a BAR dependent phospho-switch in JMJD1A resulting in its recruitment to thermogenic gene chromatin that is independent of changes in H3K9 methylation. In contrast, the chronic adaptation in beige adipocytes requires both the phospho-switch dependent chromatin recruitment and H3K9 demethylation activities of JMJD1A.

The present results also provide a prototypic mechanism for how an epigenetic modifier senses chronic environmental stress via signal specific posttranslational modification (PTM) (step 1) and then re-writes epigenetic information (step 2) to induce an adaptive phenotype in response to cold stress. Signal dependent PTMs are also found in many transcription factors and co-factors that reversibly associate with chromatin through non-covalent interactions to mediate dynamic genome events (reviewed in [3, 38]). Additionally, epigenetic modifiers can also provide stable-covalent modifications of chromatin to ensure the gene expression changes in response to stress signaling are sustained over time. The mechanism described here is in response to cold-stress but it is likely that similar mechanisms are involved in adaptive changes to additional chronic environmental stresses including nutritional variation, fasting/caloric restriction, pathogen exposure, and chemical stress.

Beige fat cells also actively consume fat and glucose to contribute to whole body insulin sensitivity

and help regulate whole body energy balance. When we exposed the *Jmjd1a*-S265A$^{KI/KI}$ mice to HFD feeding followed by cold exposure, we also uncovered a unique role for JMJD1A mediated beige-ing in regulating insulin sensitivity. The phosphorylation defective knock-in mice and *WT* mice gained similar amounts of weight on the HFD and had similar responses to a GTT challenge. However, after exposure to 4ºC, mice with a S265A mutation of JMJD1A that prevents the BAR phospho-switch displayed both a hyperinsulinemic response during the GTT and had deficient glucose clearance when challenged with insulin. These responses reveal a crucial role for pS265-JMJD1A in glucose regulation only when mice are exposed to the additional stress of cold exposure on top of the-HFD challenge. However, because the mice have a global knock-in for S265A and they also show defective insulin responses in BAT and muscle, we cannot conclude that the defective insulin response is only due to the defect in scWAT beige conversion.

Induction of beige fat cells is now drawing great clinical interest in the search for therapeutic targets for metabolic disorders. The present results show that preventing phosphorylation of S265-JMJD1A results in defective thermogenesis and development of cold-dependent insulin resistance in mice, while expression of phospho-mimetic S265D-JMJD1A promotes a beige adipogenic program. Thus, S265-phosphorylation of JMJD1A might prove to be a novel molecular target for the treatment of metabolic disorders via promoting beige adipogenesis.

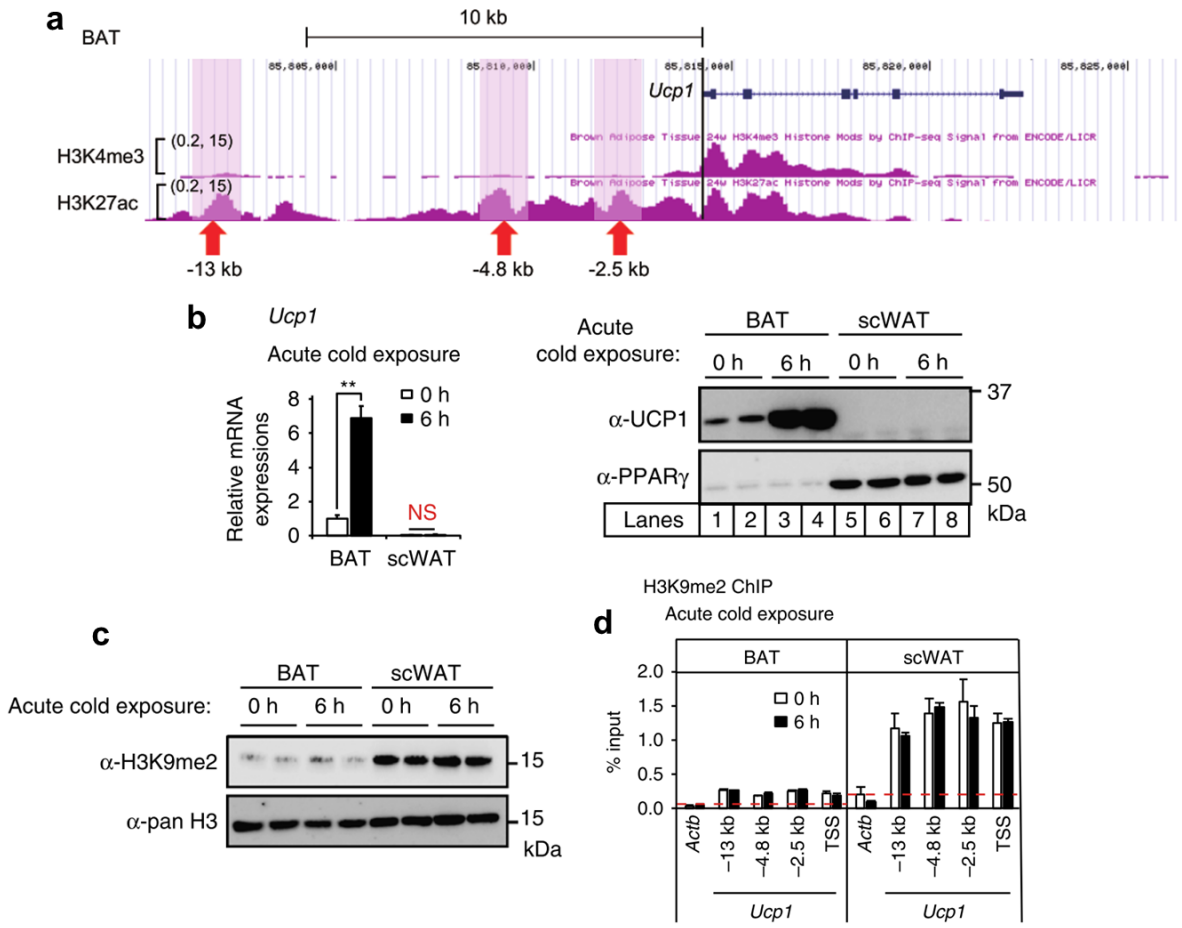

Fig.1 H3K9me2-independent thermogenic gene inductions in BAT

(**a**) ChIP-seq profiles of H3K4me3 and H3K27ac on *Ucp1* genomic region in mouse BAT were obtained from ENCODE/LICR histone modification data in the UCSC genome browser (NCBI37/mm9 assembly). Light pink shadows highlight the enhancers as we reported previously (Abe et al. 2015). Scale bar, 10kb. (**b**) *Ucp1* mRNA (n = 3) (left) and protein levels detected by immunoblotting (IB) (right) in BAT and scWAT of mice exposed to 4ºC for 6 hr. (**c**) H3K9me2 immunoblotting using purified histones from adipose tissues of mice housed at RT. (**d**) H3K9me2 ChIP-qPCR in BAT and scWAT of mice exposed to 4ºC for 6 hr (n = 3). Data are mean ± s.e.m. Student's t-test was performed for comparisons in **b**. $^{**}P < 0.01$ were considered statistically significant.

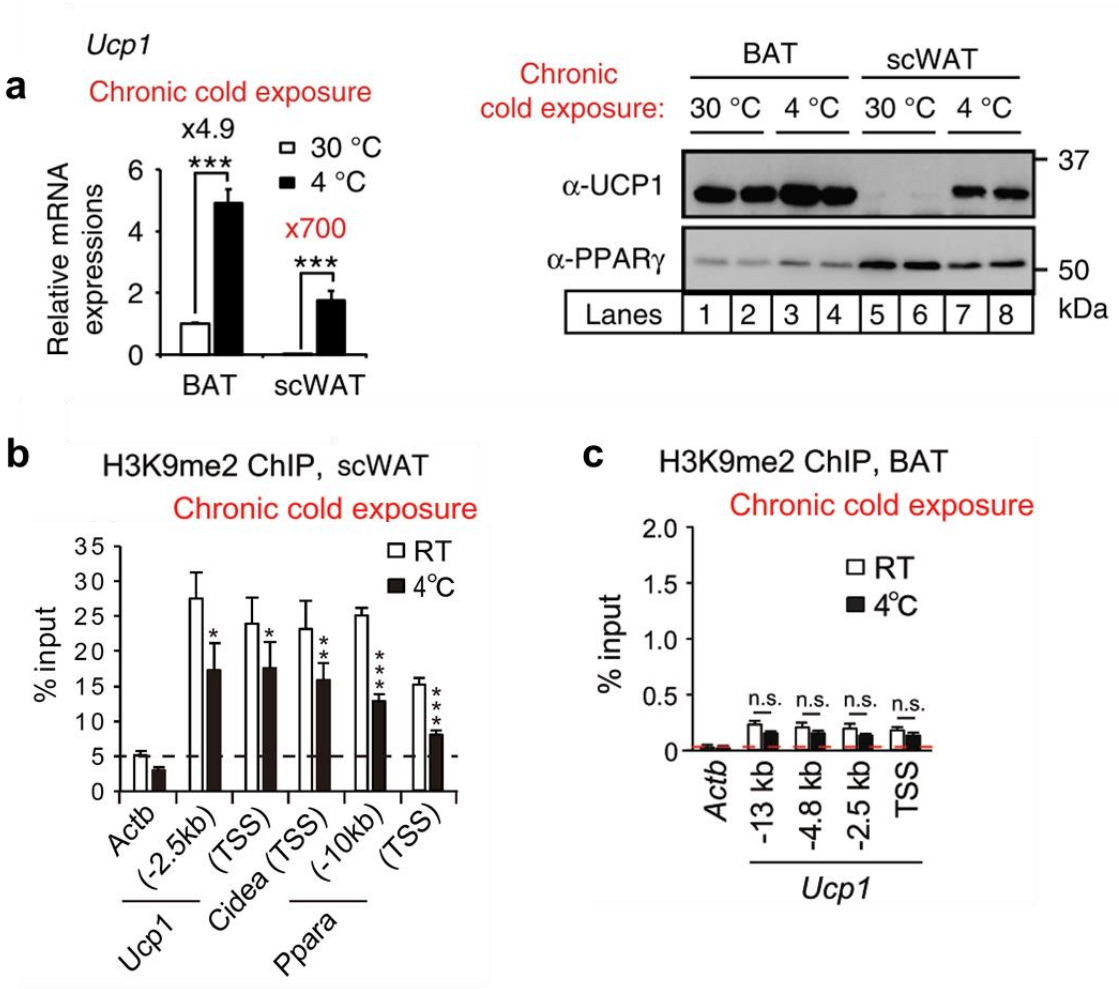

Fig.2 H3K9me2-dependent Beige-selective gene inductions in scWAT

(**a**) *Ucp1* mRNA expressions (n = 3) (left) and proteins (right) in BAT and scWAT from mice exposed to 30ºC or 4ºC for 1 week. (**b**) H3K9me2 ChIP-qPCR in scWAT from mice placed at 4ºC for 1 week (n = 4) (**c**) ChIP-qPCR showing H3K9me2 levels in BAT of mice exposed to RT or 4ºC for 1 week (7-8 week old male, n = 6). Data are mean ± s.e.m. Student's t-test was performed for comparisons in **a**,**b**. $*P < 0.05$, $**P < 0.01$ and $***P < 0.005$ were considered statistically significant.

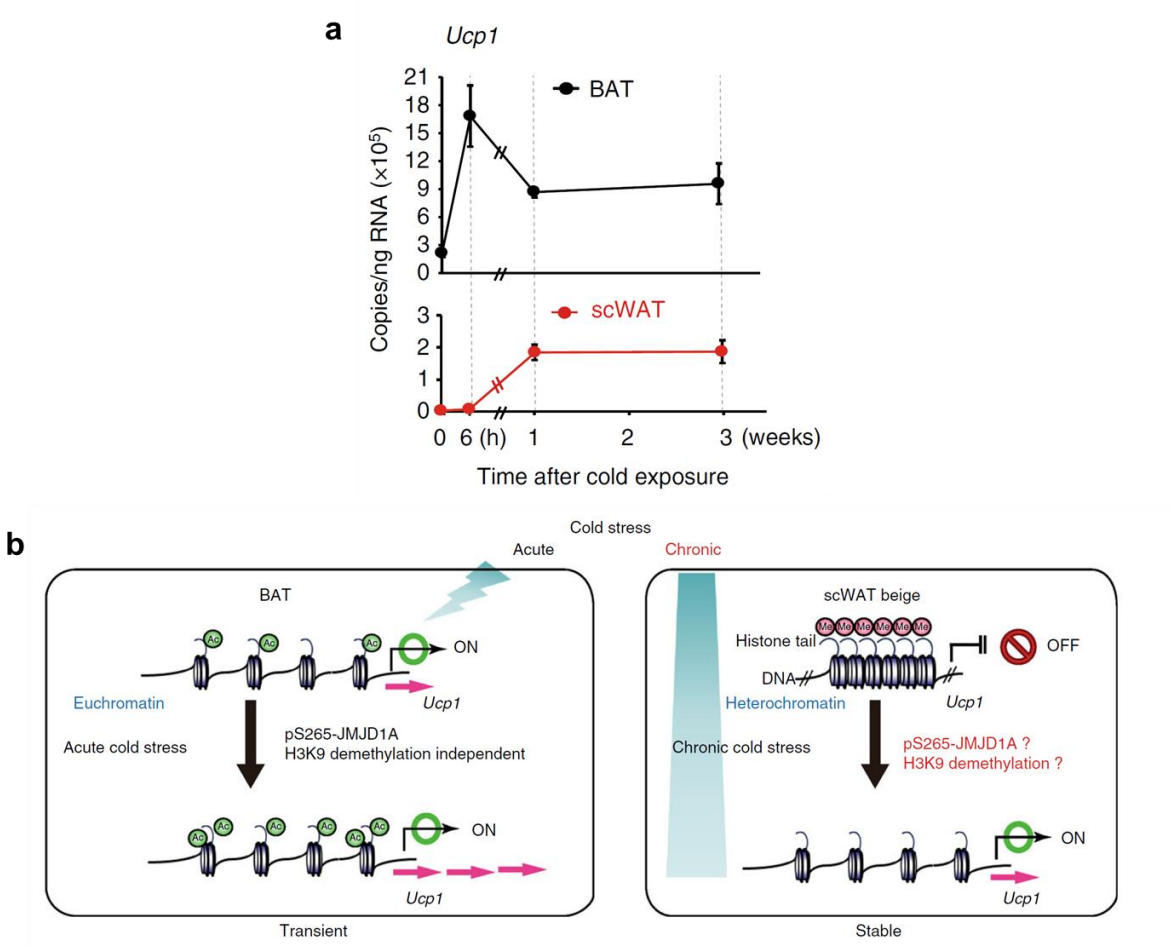

Fig.3 *Ucp1* induction in BAT and scWAT during cold exposure

(**a**) Bi-phasic *Ucp1* expressions during cold exposure in BAT and scWAT. Mice were exposed to 4ºC for the indicated time and *Ucp1* mRNAs in BAT and scWATs were quantified by qPCR (n = 3). The data were converted to copy number per ng of total RNA. (**b**) In BAT, *Ucp*1 locus is in euchromatin (left) while in scWAT it is in heterochromatin with H3K9me2 (right). In BAT, cold exposure leads acute induction of *Ucp1* mRNA through the mechanisms independent of H3K9me2 demethylation (left). In scWAT, H3K9me2 at *Ucp1* gene locus needs to be removed for beige adipogenesis (right bottom) Data are mean ± s.e.m.

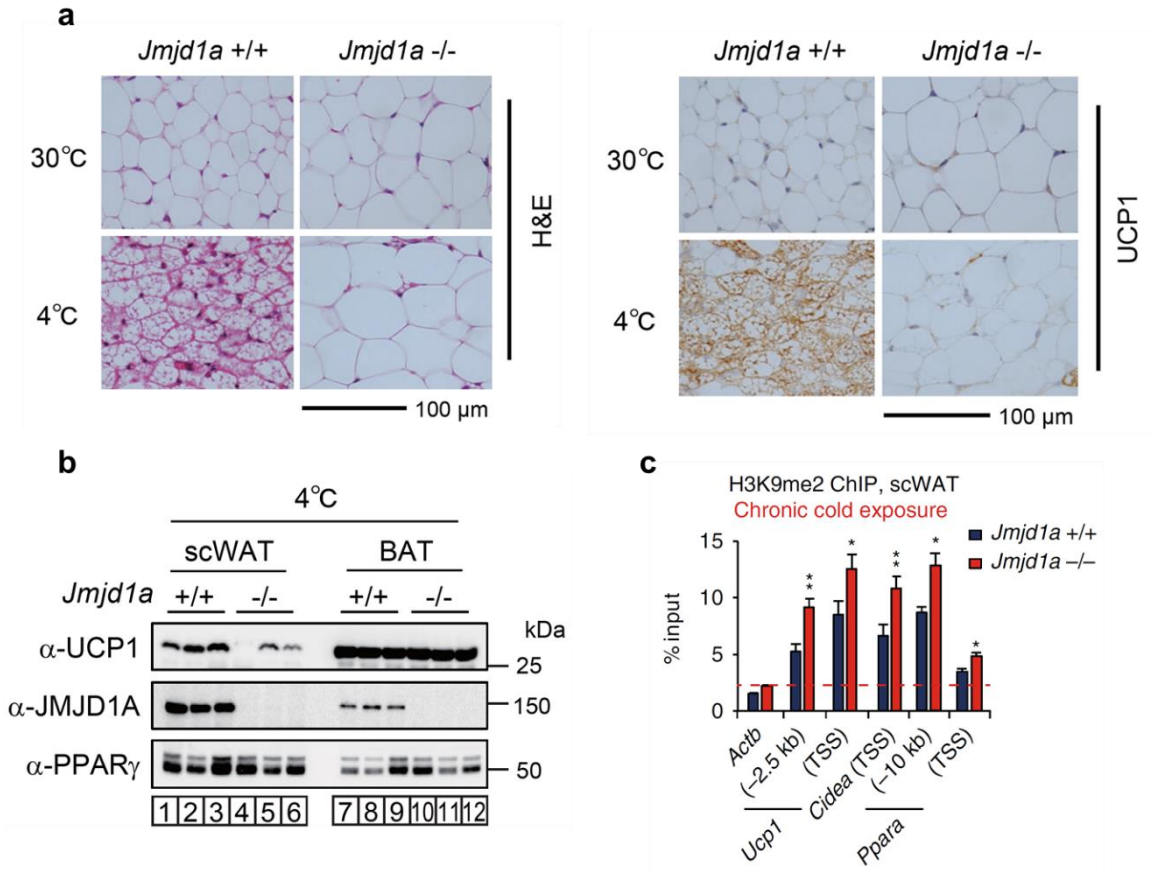

Fig.4 JMJD1A induces beige-selective genes

(**a**) Hematoxylin and eosin (H&E) and UCP1 staining sections of scWATs from *WT* (+/+) and *Jmjd1a*-null (-/-) mice exposed to 30ºC or 4ºC for 1 week (left and middle panels) (bar, 100 μm).

(**b**) Tissue homogenate of scWATs and BAT from these mice exposed to 4ºC were subjected to immunoblot analysis with anti-UCP1, anti-JMJD1A, or anti-PPARγ (right). (**c**) H3K9me2 ChIP-qPCR on beige-selective genes using scWAT from age-matched *WT* (+/+) and *Jmjd1a*-null (-/-) mice placed at 4ºC for 1 week (n = 4 per genotype group). Data are mean ± s.e.m. Student's t-test was performed for comparisons in **c**. $*P < 0.05$, $**P < 0.01$ were considered statistically significant.

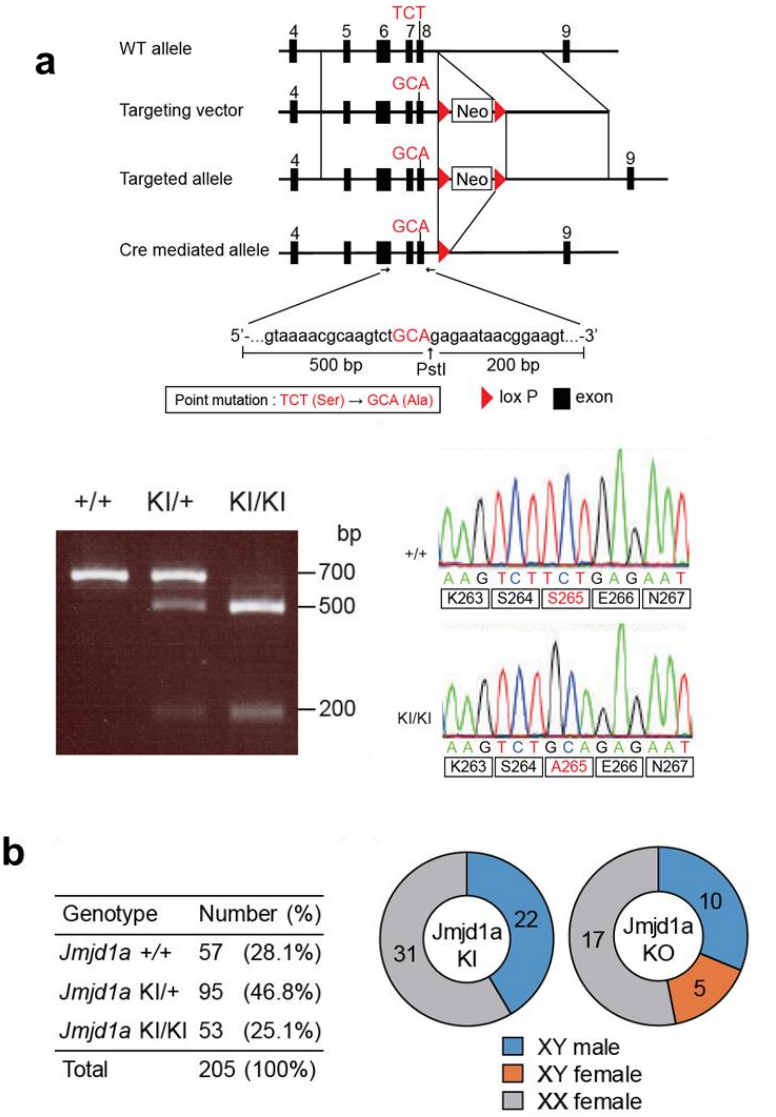

Fig. 5 Generation of *Jmjd1a*-S265A$^{KI/KI}$ mice

(**a**) Top: Schematic diagram of the targeting strategy of S265A mutation. Only the relevant restriction sites are indicated. Locations of the PCR primers (arrows) for genotyping are shown. Right bottom: An ethidium bromide-stained agarose gel illustrates PCR products for genotyping *WT*, *Jmjd1a*-S265AKI/+ mice, and *Jmjd1a*-S265AKI/KI mice. Left bottom: Direct sequencing of genomic DNA from mice distinguishes between *WT* (+/+) mice (Serine 265: TCT) and *Jmjd1a*-S265AKI/KI mice (Alanine 265: GCA). (**b**) Genotype in pups (n = 205) obtained by crossing *Jmjd1a*-S265AKI/+ mice. Quantification of XY male, XY female, and XX female (left panel).

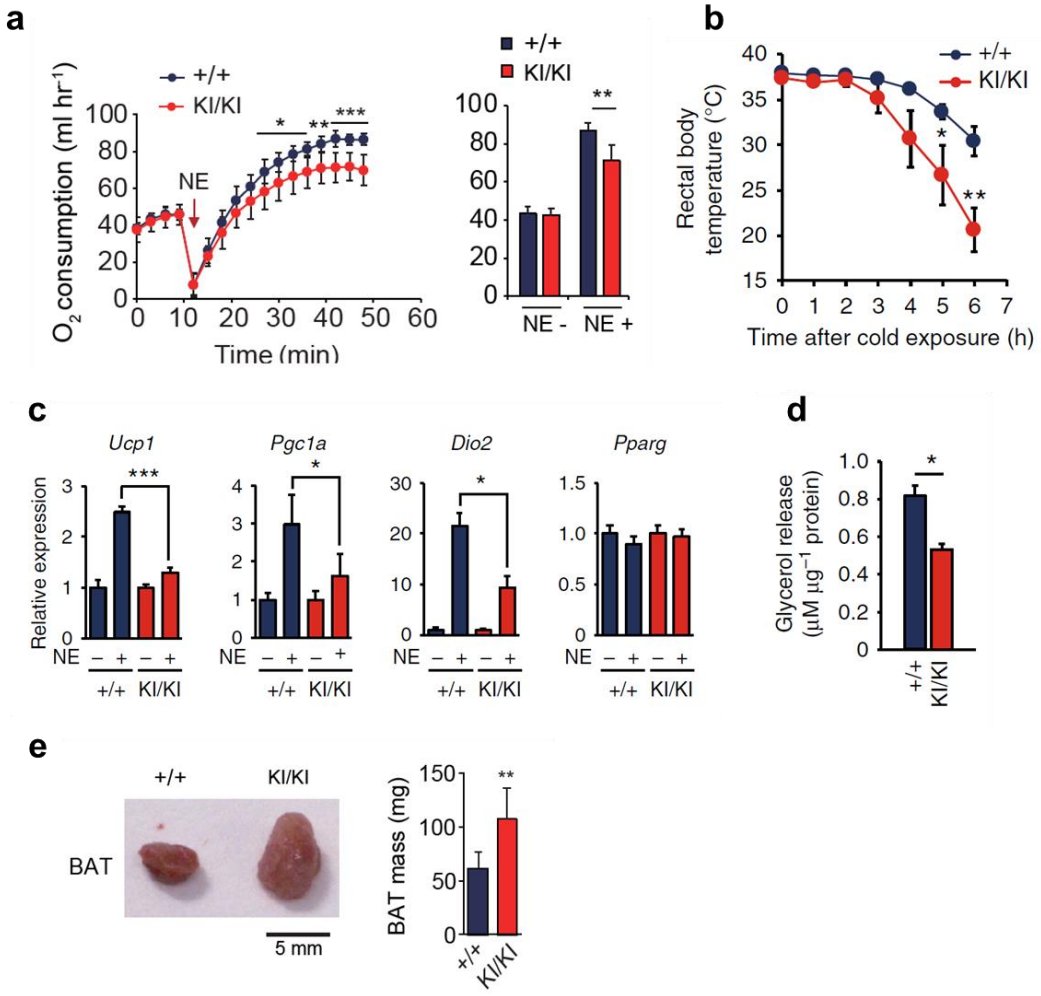

Fig. 6 *Jmjd1a*-S265A$^{KI/KI}$ mice reduced BAT thermogenic activity

(**a**) Norepinephrine (NE, 1 mg/kg BW)-induced changes in O2 consumption of *WT* and *Jmjd1a*-S265AKI/KI mice acclimated to 30ºC for 2 weeks (left). O2 consumption rates before and 30 min after NE treatment were analyzed (right) (n = 6/group). (**b**) Cold intolerance in *Jmjd1a*-S265A$^{KI/KI}$ mice (n = 6 per genotype group). Shown is the body temperature of 9-week-old mice at different times after cold exposure (4ºC). (**c**) Impaired NE-induced activation of BAT selective genes in BAT (n = 6 per genotype group). (**d**) Reduced NE-induced NE-induced glycerol release in primary brown adipocytes from *Jmjd1a*-S265A$^{KI/KI}$ mice. (**e**) Representative images (bar, 5 mm) (left) and the weights (right) of BAT of aged *WT* (+/+) and *Jmjd1a*-S265AKI/KI mice (n = 6/group). Data are mean ± s.e.m. Tukey's post hoc comparison in **c.** Student's t-test was performed for comparisons in **a,b,d,e**. *$P < 0.05$, **$P < 0.01$ and ***$P < 0.005$ were considered statistically significant.

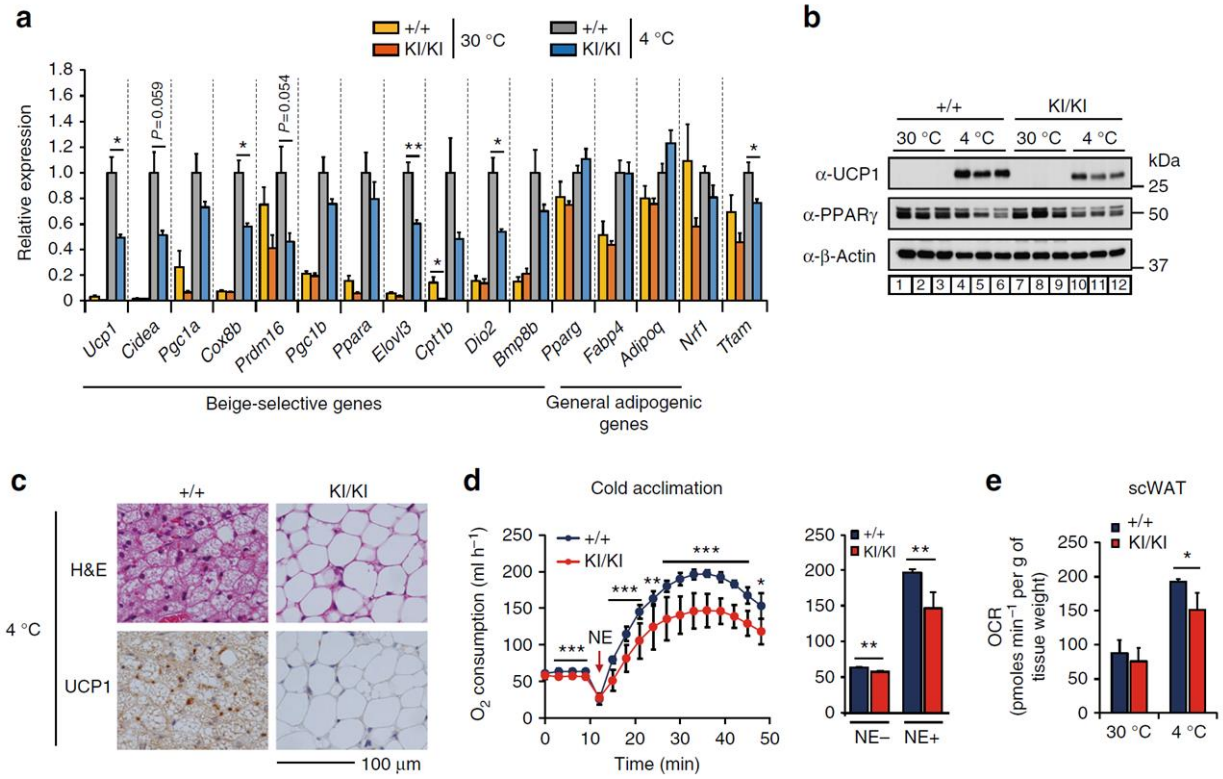

Fig. 7 S265 phosphorylation of JMJD1A induces beige-selective genes

(**a**) qPCR analysis demonstrates decreased expression of beige-selective genes in scWAT from *Jmjd1a*-S265A$^{KI/KI}$ mice exposed to 30ºC or 4ºC for 1 week (n = 5 per genotype group). (**b**) Immunoblot analysis of UCP1 and PPARγ in tissue homogenates of scWAT from mice presented in **a**. (**c**) Haematoxylin and eosin (H&E) and UCP1 staining sections of scWAT from *WT* and *Jmjd1a*-S265A$^{KI/KI}$ mice exposed to chronic cold exposure (4ºC for 1 week) (bar, 100 µm). (**d**) NE-induced oxygen consumption rate (OCR) in mice exposed to chronic cold exposure (4ºC for 4 weeks) (n = 7 per genotype group) (left). OCR before and 30 min after NE treatment are analyzed (right) (n = 7). (**e**) OCR of scWAT from mice exposed to 30ºC or 4ºC for 1 week (*WT*: n=3, *Jmjd1a*-S265A$^{KI/KI}$: n = 4). Data are mean ± s.e.m. Tukey's post hoc comparison in **a**. Student's t-test was performed for comparisons in **d**,**e**. **P* < 0.05, ***P* < 0.01 and ****P* < 0.005 were considered statistically significant.

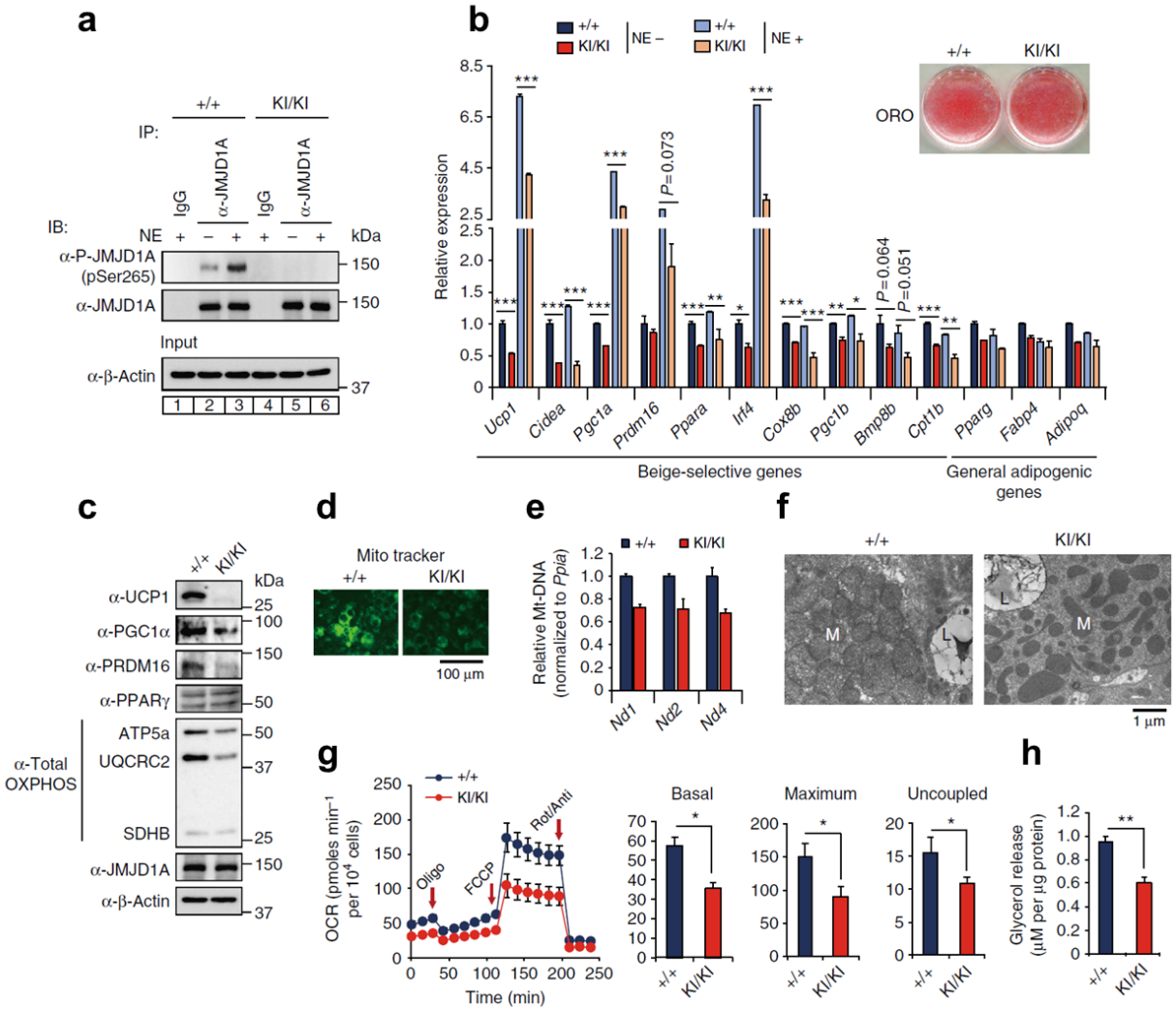

Fig. 8 pS265-JMJD1A cell autonomously induces beige-selective genes

(**a**) pSer265-JMJD1A protein levels in *WT* (+/+) and S265A knock-in whole-cell lysates (WCL) from scWAT cultures treated with NE or vehicle for 1 hr. (**b**) Decreased beige-selective gene expressions in S265A knock-in scWAT cultures treated with NE (10 μM) for 2 hr (mean ± s.e.m. of three technical replicates). ORO staining of indicated genotype of scWAT cultures (inset). (**c**) Immunoblot analysis using anti-UCP1, anti-PGC1α, anti-PRDM16, anti-PPARγ, or anti-total OXPHOS antibodies cocktail using WCL from WT and S265A knock-in scWAT cultures. (**d**) Mito Tracker staining in indicated genotype scWAT cultures (bar, 100 μm). (**e**) Mitochondrial DNA (mt-DNA) contents measured by qPCR in indicated scWAT cultures (mean ± s.e.m. of three independent experiments). (**f**) Electron micrographs of indicated genotype of scWAT cultures (bar, 1 μm). Mitochondria (M) and lipid droplets (L) are indicated. (**g**) The OCR of indicated scWAT cultures (left). The arrows indicate time

of addition for oligomycin (Oligo), FCCP, and rotenone/antimycin A (Rot/Anti). Basal, maximum, and uncoupled respiration were calculated (mean ± s.e.m. of five technical replicates) (right). (**h**) Glycerol release from indicated scWAT cultures after the treatment with NE for 3 hr (mean ± s.e.m. of three independent experiments). Student's t-test was performed for comparisons in **b**,**g,h**. **P* < 0.05, ***P* < 0.01 and ****P* < 0.005 were considered statistically significant.

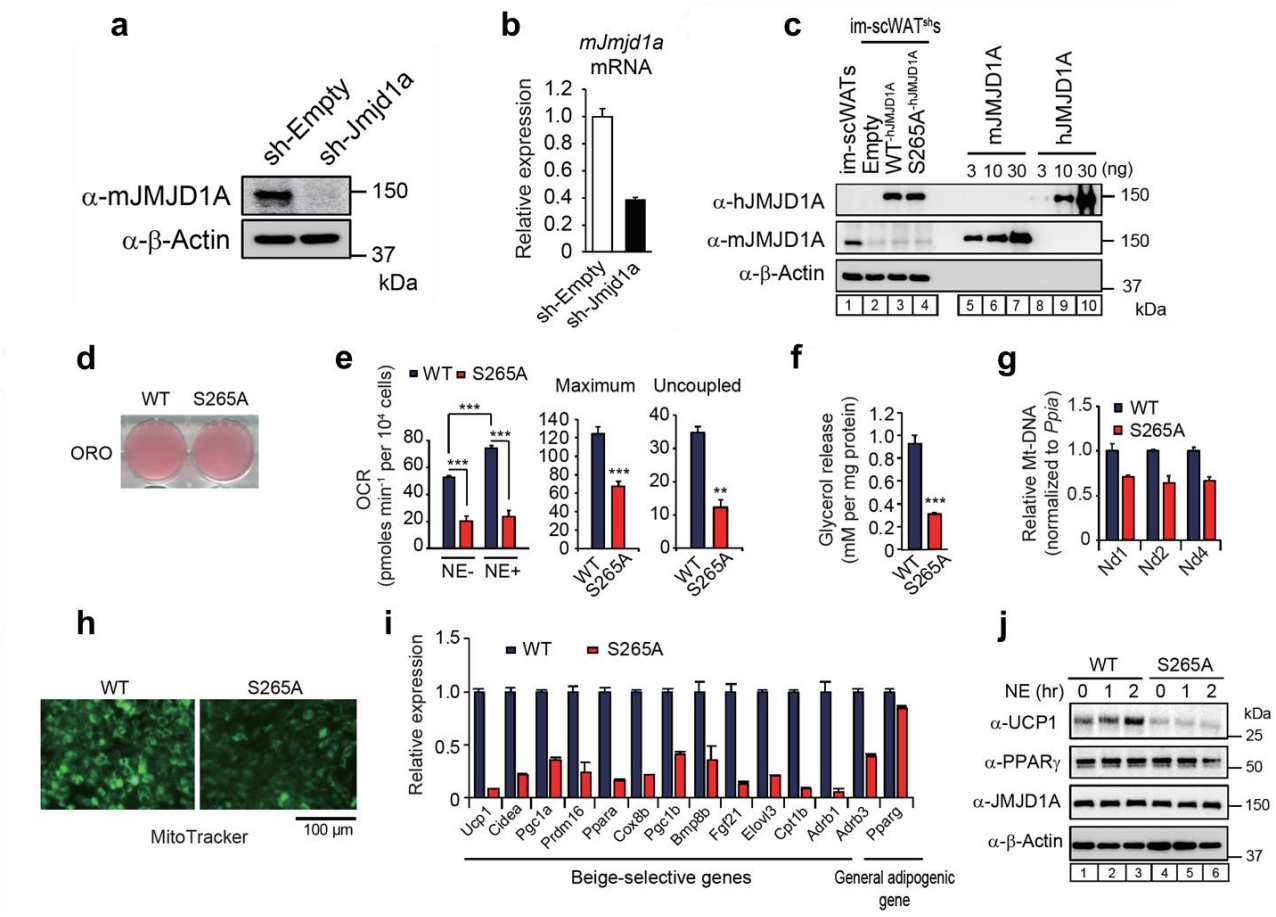

Fig. 9 Establishment of S265A-JMJD1A immortalized preadipocyte

(**a**) Immunoblot and (**b**) qPCR analysis (right). The mRNA values are depicted relative to mRNA in im-scWATs (sh-Empty), which are arbitrarily defined as 1. Data are mean ± s.e.m. of three technical replicates. (**c**) Exogenous human JMJD1A expression level in im-scWATs was similar level to native JMJD1A in im-scWATs. Aliquots of whole cell lysate prepared from im-scWATs, im-scWATs knocked-down Jmjd1a by shRNA (im-scWATs) overexpressing WT or S265A human JMJD1A, or control Zeor-empty (Empty) along with the indicated amounts of recombinant purified human JMJD1A (full length) or His-tagged mouse JMJD1A (full length) proteins were subjected to IB analysis with anti-mJMJD1A antibody or anti-hJMJD1A antibody. (**d**) Oil red O (ORO) staining. (**e**) The metabolic profile of WT- and S265A-hJMJD1A-transduced im-scWATs differentiated with ROS assessed by a Seahorse XF24 extracellular flux analyzer. The parameters analyzed on the same plate are represented as norepinephrine (NE, 10 μM)-induced mitochondrial respiration (left), maximum mitochondrial respiration (middle) and uncoupled mitochondrial respiration (right) (mean ± s.e.m. of five technical

replicates). (**f**) Glycerol release in WT- and S265A-hJMJD1A-transduced im-scWATs treated with NE (10 μM) for 2 hr (mean ± s.e.m. of three independent experiments). (**g**) Mitochondrial DNA (Mt-DNA) content. The mt-DNA values are depicted relative to mt-DNA in WT-hJMJD1A-transduced im-scWATs, which are arbitrarily defined as 1 (mean ± s.e.m. of three independent experiments). (**h**) Mito Tracker staining in WT- and S265A-hJMJD1A-transduced im-scWATs (bar, 100 μm). (**i**) mRNA levels of beige-selective genes and general adipogenic gene in WT- and S265A-hJMJD1A-transduced im-scWATs differentiated with rosiglitazone were measured by qPCR. The mRNA values are depicted relative to mRNA in WT-hJMJD1A-transduced im-scWATs, which are arbitrarily defined as 1 (mean ± s.e.m. of three technical replicates). (**j**) Immunoblot analysis of UCP1, PPARγ and JMJD1A in the time course of norepinephrine (NE, 10 μM) treatment in WT- and S265A-hJMJD1A-transduced im-scWATs differentiated with rosiglitazone. Equal loading of the proteins was confirmed by β-actin.
$^{**}P < 0.01$ and $^{***}P < 0.005$ were considered statistically significant.

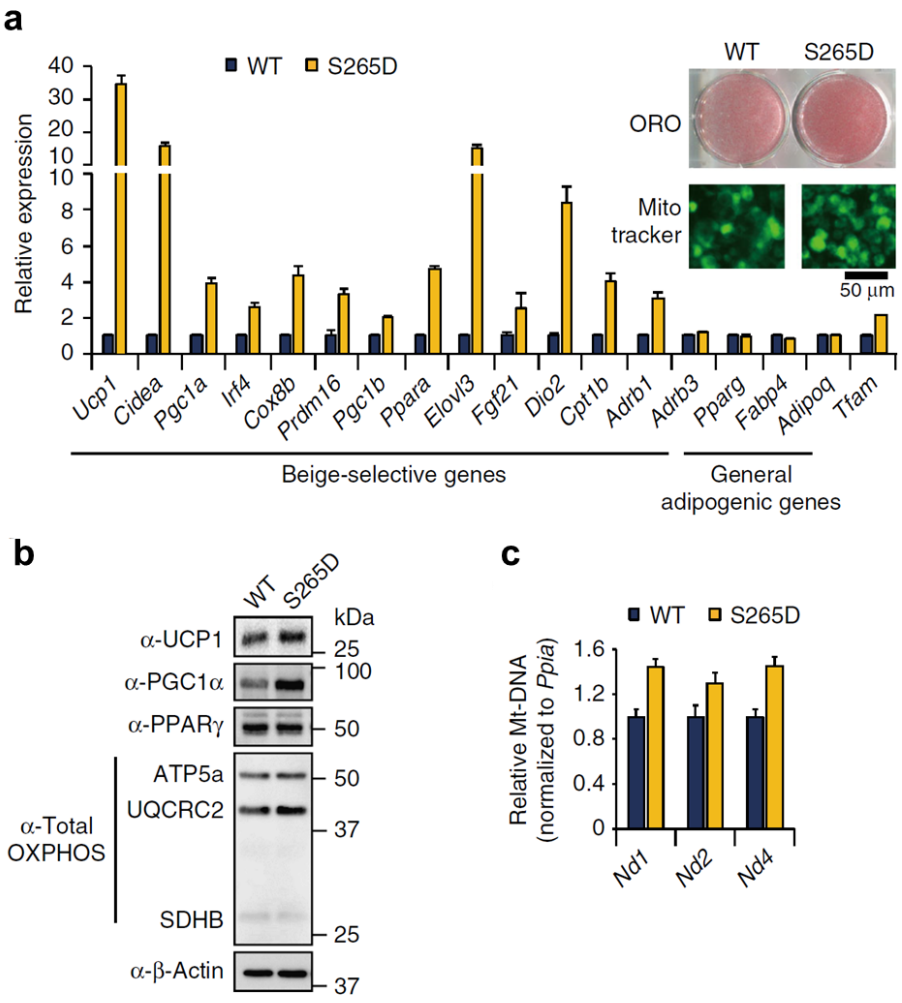

Fig. 10 Phosphomimetic S265D-JMJD1A induces beige-selective genes

(**a**) Increased expressions of beige-selective genes in S265D$^{\text{-hJMJD1A}}$-transduced im-scWATs (mean ± s.e.m. of three technical replicates). ORO staining and Mito Tracker staining (inset) (bar, 50 μm). (**b**) Immunoblotting with anti-UCP1, anti-PGC1α, anti-PPARγ, or anti-total OXPHOS antibodies cocktail using WCL from indicated im-scWATs. (**c**) Mitochondrial DNA content measured by qPCR in indicated im-scWATs (mean ± s.e.m. of three technical replicates).

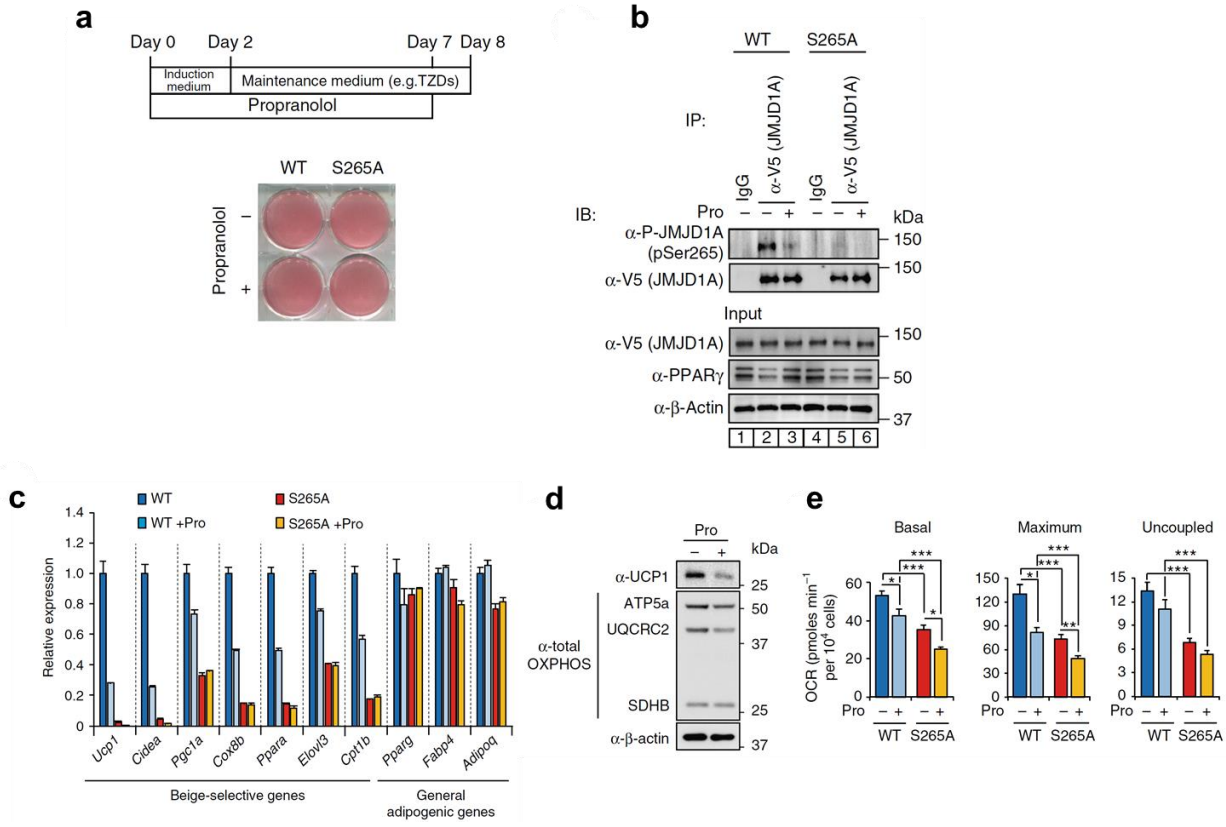

Fig. 11 TZD-induced beige adipogenesis is mediated by p-JMJD1A

(**a**) WT^{-} or S265A$^{-hJMJD1A}$-transduced im-scWATs were differentiated for beige adipogenesis in the presence or absence of propranolol (Pro) as schematically illustrated (top) and ORO staining was performed (bottom). (**b**) Whole-cell lysates (WCL) from WT^{-} or S265A$^{-hJMJD1A}$-transduced im-scWATs differentiated under Pro (100 nM) plus or minus condition were subjected to immunoprecipitation (IP) with anti-V5 antibody followed by immunoblot (IB) analysis with anti-P-JMJD1A (pSer265) antibody. (**c**) qPCR analysis of beige-selective genes and general adipogenic genes in WT^{-} or S265A$^{-hJMJD1A}$-transduced im-scWATs under Pro plus or minus condition (mean ± s.e.m. of three technical replicates). (**d**) Immunoblotting with anti-UCP1 or anti-total OXPHOS antibodies cocktail using WCL from indicated viral transduced im-scWATs differentiated under Pro plus or minus condition. (**e**) OCRs (basal, maximum, and uncoupled) of WT^{-} or S265A$^{-hJMJD1A}$-transduced im-scWATs differentiated under Pro plus or minus condition. Data are mean ± s.e.m. of five technical replicates. Analysis of variance were performed followed by Tukey's post hoc comparison in **e**. *P< 0.05, **P< 0.01 and ***P< 0.005 were considered statistically significant.

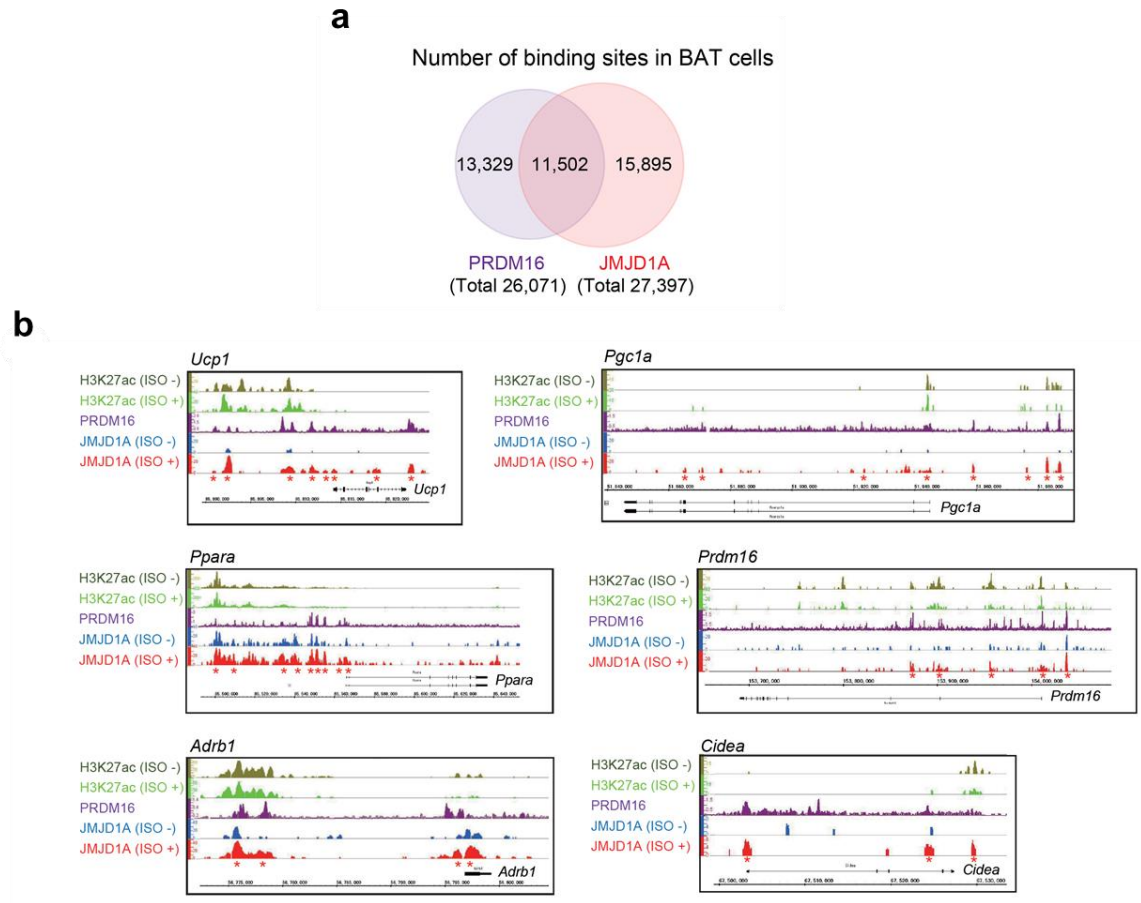

Fig. 12 PRDM16 shares binding sites on beige-selective genes with JMJD1A

(**a**) Venn diagram shows the number of genome-wide DNA binding sites of PRDM16 and JMJD1A in brown adipocytes following the stimulation with β-adrenergic agonist, isoproterenol (ISO). (**b**) ChIP-seq profiles for H3K27ac, PRDM16 and JMJD1A in brown adipocytes treated with or without β-adrenergic agonist, isoproterenol (ISO, 1 μM for 2 hr) on beige-selective genes. Red asterisks indicate ISO-dependent JMJD1A binding sites overlapped with those of PRDM16. Data for JMJD1A, H3K27ac and PPARγ were obtained from Abe et al., 2015 (Nat Commun 6, 7052 (2015)) and PRDM16 from Harms et al., 2015 (Genes Dev 29, 298-307 (2015)) in **a**, **b**.

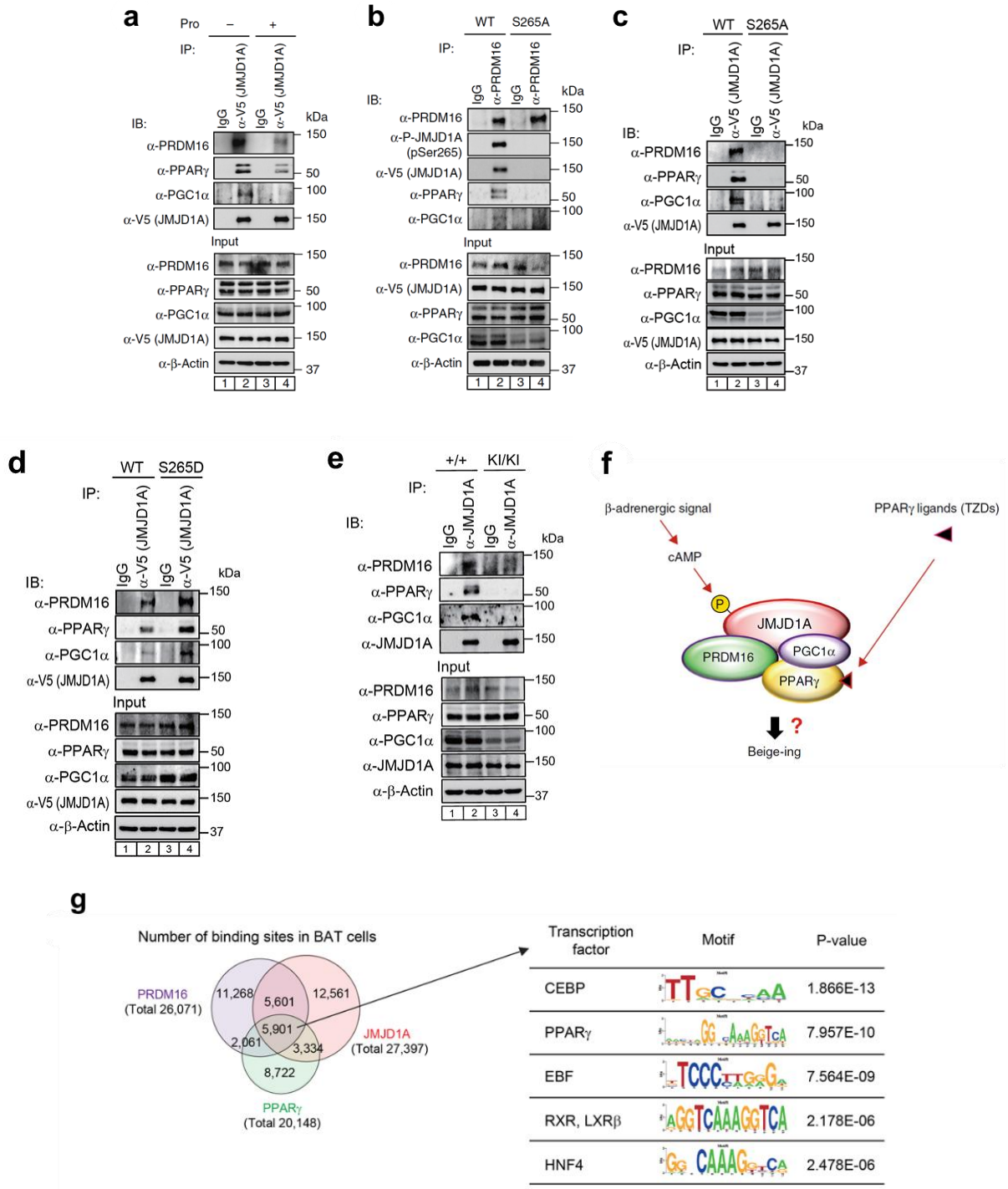

Fig. 13 pS265-JMJD1A-PPARγ-PGC1α-PRDM16 protein complex

(**a,b**) Immunoblotting with anti-PRDM16, anti-P-JMJD1A, anti-V5, anti-PPARγ, or anti-PGC1α

antibody following immunoprecipitation with anti-PRDM16 antibody (**a**) or with anti-V5 antibody for JMJD1A (**b**) from WCL of differentiated WT^{-} or S265A$^{-hJMJD1A}$-transduced im-scWATs. (**c,d**) Whole-cell lysates (WCL) from WT-, S265A- (**c**) or S265D-^{hJMJD1A} (**d**)-transduced im-scWATs were subjected to immunoprecipitation (IP) with anti-V5 antibody followed by immunoblot (IB) analysis with either anti-PRDM16, PPARγ, PGC1α or V5 antibodies. (**e**) WCL from WT (+/+) and Jmjd1a-S265AKI/KI scWAT cultures was subjected to immunoprecipitation (IP) using anti-JMJD1A antibody and immunoblotted (IB) with either anti-PRDM16, PPARγ, PGC1α or JMJD1A antibodies. Uncropped images of the blots. (**f**) Schematic drawing of p265-JMJD1A-PPARγ-PGC1α-PRDM16 protein complex. Integration of β-adrenergic-cAMP signaling and the PPARγ ligand binding is mediated by JMJD1A through a mechanism where pS265-JMJD1A forming a complex with PGC1α, PRDM16, and PPARγ to mediate expressions of beige-selective genes. (**g**) Venn diagram shows the number of genome-wide DNA binding sites of PRDM16, JMJD1A and PPARγ in brown adipocytes treated with ISO (left panel). Transcription factor binding motifs enriched in genomic regions within JMJD1A, PRDM16 and PPARγ bindings are listed in the right panel. Data for JMJD1A, H3K27ac and PPARγ were obtained from Abe et al., 2015 (Nat Commun 6, 7052 (2015)) and PRDM16 from Harms et al., 2015 (Genes Dev 29, 298-307 (2015)).

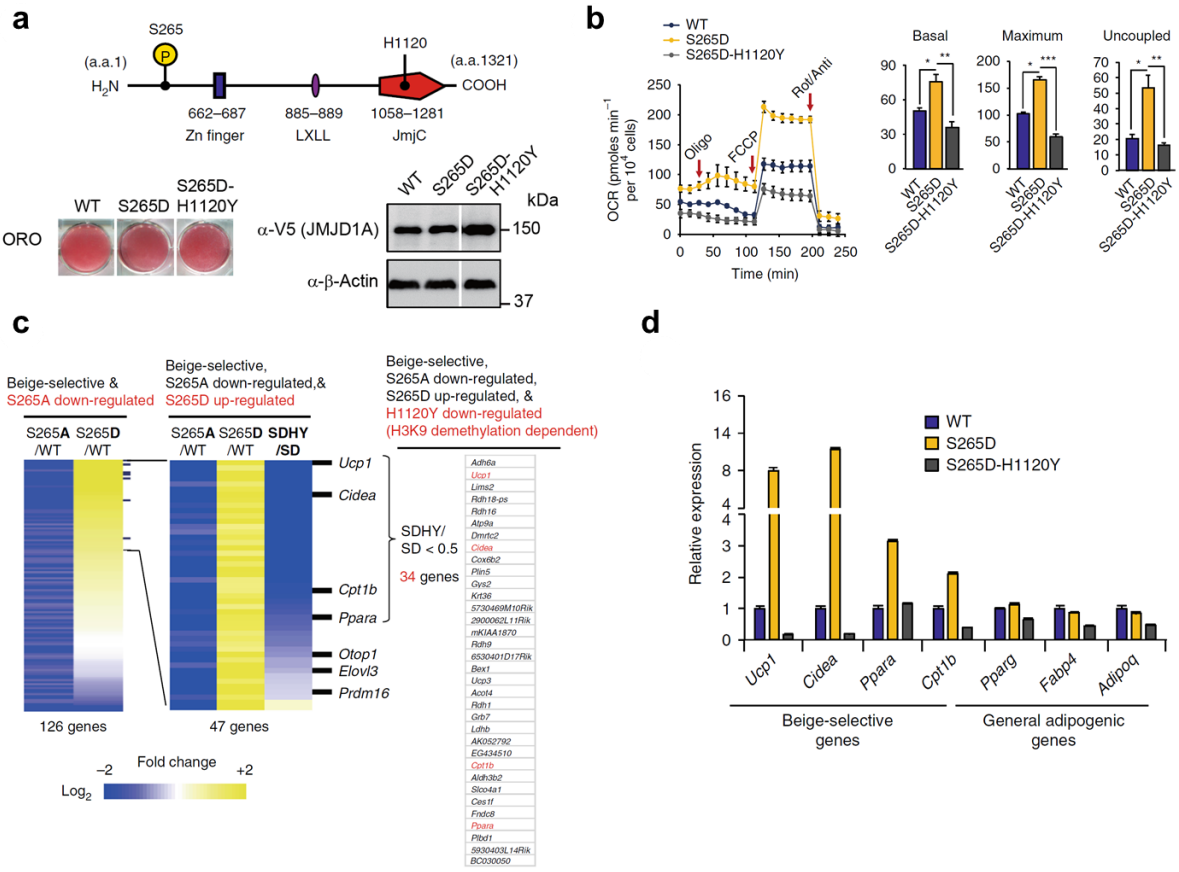

Fig. 14 Demethylation by JMJD1A is pivotal for beige adipogenesis

(**a**) Schematic representation of the domain structure of human JMJD1A. Phosphorylation site at S265 and Fe (II) binding site at H1120 are shown (Top). ORO staining in WT, S265D or S265D-H1120Y-hJMJD1A-transduced im-scWATs differentiated with rosiglitazone (left bottom). Whole-cell lysates from WT, S265D S265D-H1120Y-^{hJMJD1A}-transduced im-scWATs differentiated with rosiglitazone were subjected to immunoblot analysis with anti-V5 antibody (right bottom). (**b**) OCR in im-scWATs stably expressing WT^{-}, S265D^{-}, or S265D-H1120Y$^{-hJMJD1A}$ treated with sequentially with oligomycin (Oligo), FCCP, and rotenone/antimycin A (Rot/Anti) (left). Basal, maximum, and uncoupled respiration calculated from left (right). Data are mean ± s.e.m. of three technical replicates in a representative experiment. Analysis of variance were performed followed by Tukey's post hoc comparison. $^{*}P < 0.05$, $^{**}P < 0.01$ and $^{***}P < 0.005$ were considered statistically significant. (**c**) Heat map of mRNA levels determined by RNA-seq analysis of indicated WT or mutant versions of hJMJD1A expressing im-scWATs. Changes are $\log_2$ expression (FPKM) ratios. For reference, a color intensity scale is included. Thirty-four gene that are beige selective, S265A down-regulated, S265D

up-regulated and H1120Y down-regulated (H3K9 demethylation dependent) are listed (right). (**d**) qPCR analysis confirming RNA seq shown in **c**. Mean ± s.e.m. of three technical replicates.

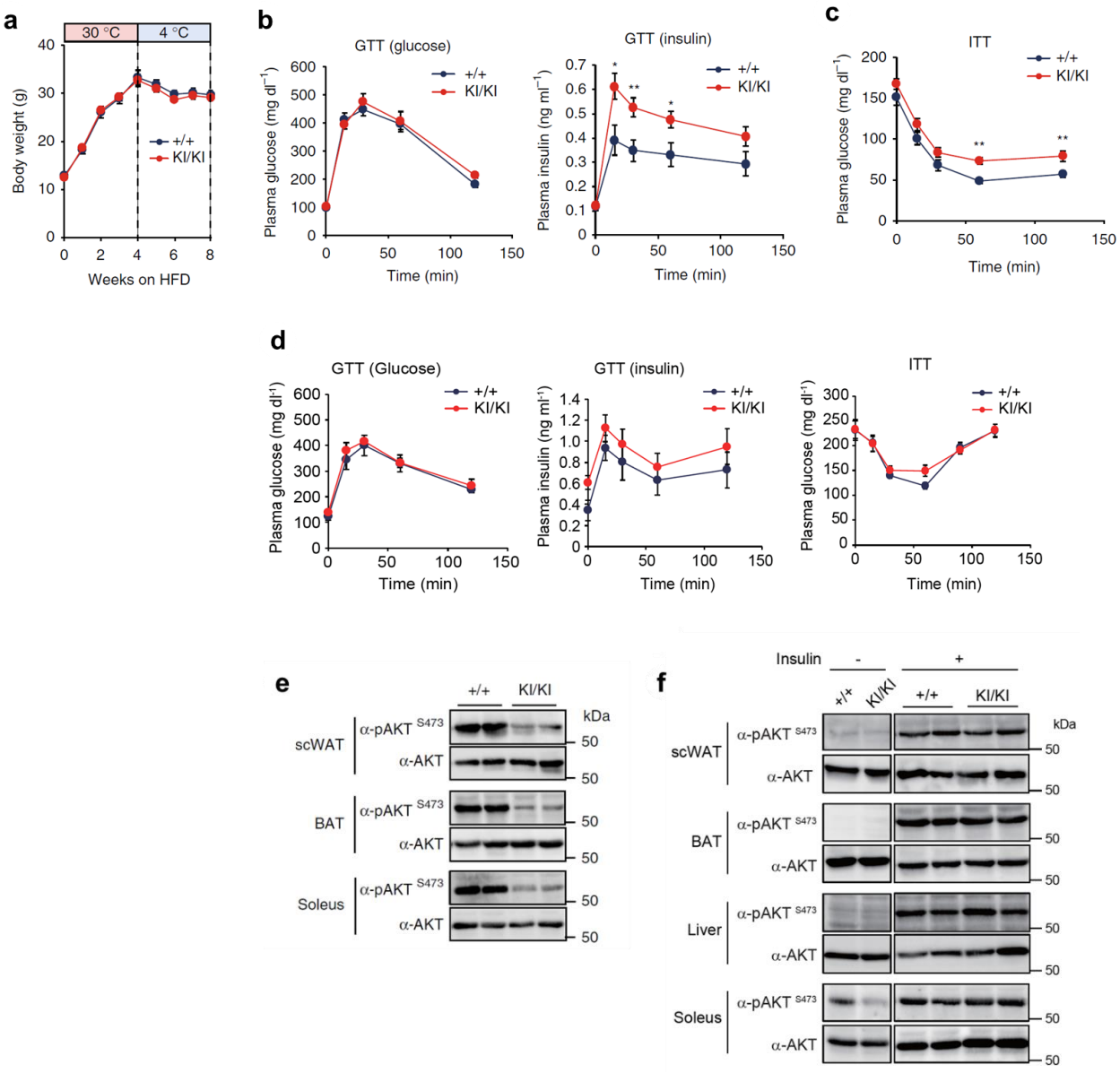

Fig. 15 Insulin resistance phenotype of *Jmjd1a*-S265A$^{KI/KI}$ mice

(**a**) Body weight changes. *WT* (+/+) and *Jmjd1a*-S265A$^{KI/KI}$ mice (*WT*: n = 6, *Jmjd1a*-S265A$^{KI/KI}$: n = 8) were fed on HFD for 4 weeks at 30ºC and then switched to 4ºC for 4 weeks. (**b**,**c**) Glucose tolerance test (GTT) (**b**) and insulin tolerance test (ITT) (**c**) in each genotype group mice fed on HFD after cold acclimation in **a** (*WT*: n = 6, *Jmjd1a*-S265A$^{KI/KI}$: n = 7). (**d**) Glucose tolerance test (GTT) and insulin tolerance test (ITT) were performed in *WT* (+/+) and *Jmjd1a*-S265AKI/KI mice fed on a high fat diet (HFD) before cold acclimation (n = 6-7/group). Plasma glucose levels (left panel) and plasma insulin levels (middle panel) during GTT

and plasma glucose levels (right panel) during ITT are shown. (**e**) Assessment of insulin signaling as quantified by the phosphorylation of AKT-S473, in scWAT, BAT or soleus from each genotype mice fed on HFD after cold acclimation presented in **a**. (**f**) Assessment of insulin signaling, as quantified by the phosphorylation of AKT-S473, in scWAT, BAT, liver or soleus muscle from *WT* and *Jmjd1a*-S265AKI/K mice housed at room temperature before and 10 min after insulin injection (0.03 unit). Data are mean ± s.e.m. (**a**-**d**). Student's t-test was performed for comparisons in **a**,**b**,**c**. **P* < 0.05 and ***P* < 0.01 were considered statistically significant.

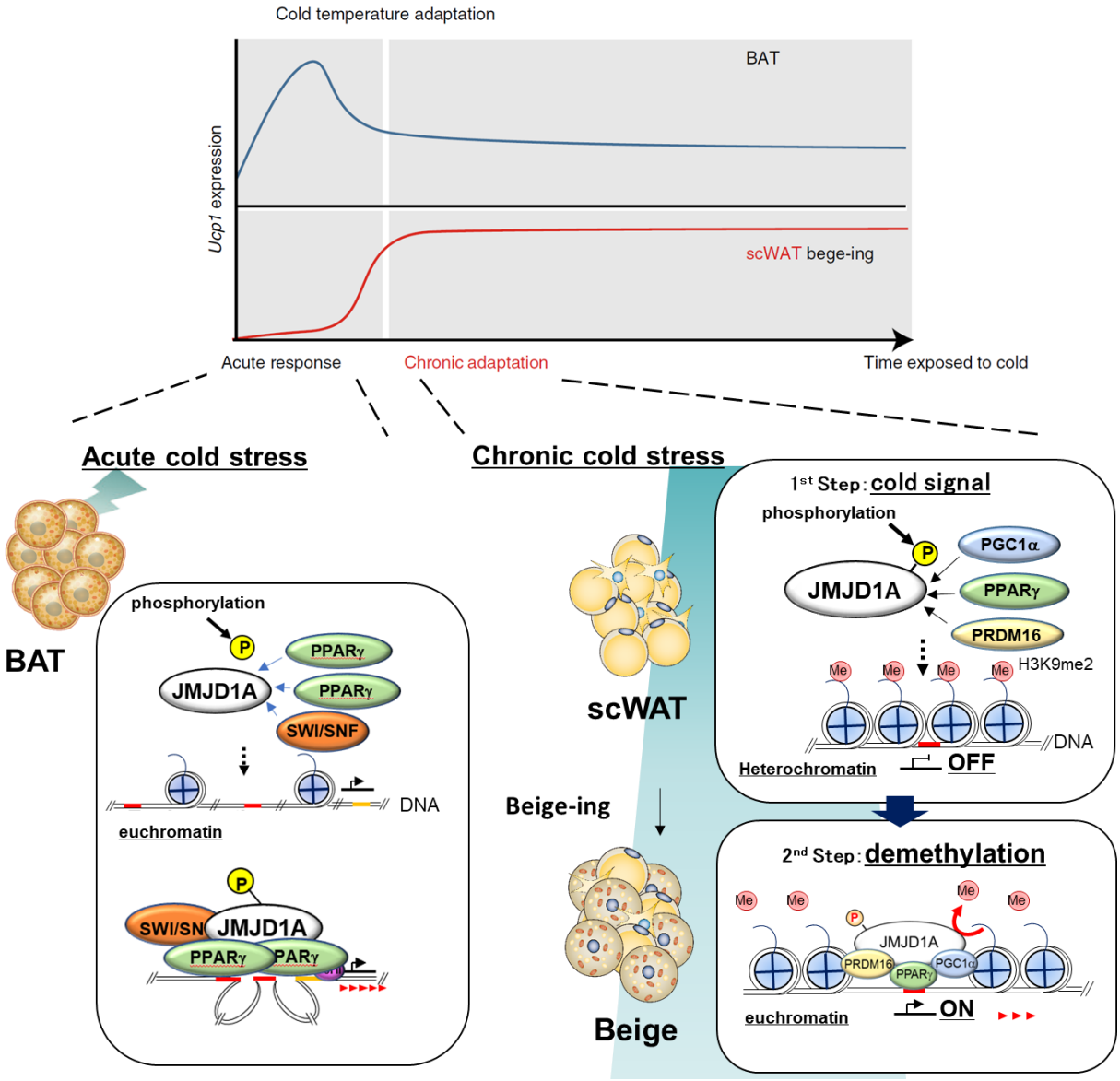

Figure 16. Mechanisms for thermogenic gene induction in acute and chronic cold stress via overlapping but distinct mechanisms of JMJD1A.

Table 1 Details of the age and sex of mice

Mouse strain	Sex	Age (weeks at starting point of the treatment)	Figure
C57BL/6N	Male	6	Figure 1b,c
	Male	16	Figure 1d
	Male	8	Figure 2a
	Male	6	Figure 2b
	Male	6-10	Figure 3a
WT and Jmjd1a-S265A$^{KI/KI}$	Male	8-9	Figure 6a
	Male	8-9	Figure 6b
	Male	7-8	Figure 6c
	Male	44	Figure 6e
	Female	16-17	Figure 7a,b
	Male	22	Figure 7c
	Female	8-9	Figure 7d
	Male	7	Figure 7e
	Male	5	Figure 15a-c,e
	Male	7-9	Figure 15d
WT (+/+) *and Jmjd1a*-null (-/-)	Male	13	Figure 4a,b
	Female	6-11	Figure 4c

Table 2 Antibodies

Antibody		Source	Catalog No /Clone No	Dilutions or concentrations
anti-mouse JMJD1A	Monoclonal	Our laboratory	IgG-F0618	5 μg mL^{-1} for IB, 10 μg mL^{-1} for IP
anti-mouse JMJD1A	Monoclonal	Our laboratory	IgG-F0231	25 μg mL^{-1} for ChIP (together with 25 μg mL^{-1} of IgG-F0618)
anti-human JMJD1A	Monoclonal	Our laboratory	IgG-F1628	5 μg mL^{-1} for IB
anti-P-JMJD1A (pS265)	Polyclonal	Our laboratory	#11890-2	1:1000 for IB
anti-PPARγ	Monoclonal	Our laboratory	IgG-A3409	0.5 μg mL^{-1} for IB
anti-PPARγ	Monoclonal	Santa Cruz	sc-7273 (E-8)	4 μg mL^{-1} for ChIP (together with 4 μg mL^{-1} of IgG-A3409)
anti-PRDM16	Monoclonal	Our laboratory	IgG-F1411	5 μg mL^{-1} for IB (used in Fig. 4f (input))
anti-PRDM16	Monoclonal	Our laboratory	IgG-F1430	10 μg mL^{-1} for IP (used in Fig. 4g)
anti-PRDM16	Polyclonal	R&D Systems	AF6295	1 μg mL^{-1} for IB (used in Fig. 3c and 4f (IP ppt.) and Fig. 4g, Supplementary Fig. 4c-e)
anti-UCP1	Polyclonal	Abcam	ab10983	1:1000 for IHC
anti-UCP1	Monoclonal	R&D Systems	MAB6158	1 μg mL^{-1} for IB
anti-PGC1α	Polyclonal	Novus	1-04676	1:1000 for IB
anti-Total OXPHOS	Monoclonal	Abcam	ab110413	1.5 μg mL^{-1} for IB
anti-β-actin	Monoclonal	Sigma	A5441	1:5000 for IB
anti-V5	Monoclonal	Invitrogen	R960-25	1 μg mL^{-1} for IB, 10 μg mL^{-1} for IP
anti-H3K9me2	Monoclonal	Dr. Kimura	IgG-6D11	10 μg mL^{-1} for ChIP 2 μg mL^{-1} for IB
anti-Histone H3	Polyclonal	Abcam	ab-1791	0.05 μg mL^{-1} for IB
anti-AKT	Monoclonal	Cell Signaling	#4691	1:1000 for IB
anti-pAKT ^{S473}	Monoclonal	Cell Signaling	#4058	1:1000 for IB

Table 3 ChIP-qPCR primers

ChIP-qPCR primers			
Gene	Sequence		Amplified regions
	Forward Primer	Reverse Primer	
Actb	5'-TGAGGTACTAGCCACGAGAGAG-3'	5'-ACACCCGCCACCAGGTAAGCA-3'	*Actb* (Intron 1)
Ppib	5'-CTCACCCCAACTAGTCTAATCC-3'	5'-GTGACACACAGTGACTAACTTCC-3'	*Ppib* (Intron 3)
Ucp1	5'-GCAACCCTCTCCCATCAGTG-3'	5'-GCCTAACACCGTGCTTCTCA-3'	*Ucp1* (-13 kb)
	5'-TGCAACCCCTCACCTTTTAC-3'	5'-CTCCTTCCATCATCCCTTCA-3'	*Ucp1* (-4.8 kb)
	5'-TCACCCTTGACCACACTGAA-3'	5'-GTGAGGCTGATATCCCCAGA-3'	*Ucp1* (-2.5 kb)
	5'-TGCCAAGTCCCACTAGCAG-3'	5'-ACCCGTTAAGCCCAGATTG-3'	*Ucp1* (TSS)
Ppara	5'-TGGCCGGGAGGAACTG-3’	5'-GGCAGGGACAATCTCTTTGTG-3'	*Ppara* (-10 kb)
	5'-GGCAGTCCCTTCACCTAACC-3'	5'-TCCTCGATGCCCATTTAGTG-3'	*Ppara* (TSS)
Cidea	5'-CACCGCTTCACTTTGTCCTTT-3'	5'-GAGCACCCGGTTTGACAGT-3'	*Cidea* (-13.5 kb)
	5'-CACGCACACCTGCTTCTCTA-3'	5'-GATGTTGGTGGCTCTTGTCA-3'	*Cidea* (TSS)

Table 4 RT-qPCR primers

RT- qPCR primers		
Gene	Sequence	
	Forward Primer	Reverse Primer
Ppib #1	5'-GGAGATGGCACAGGAGGAA-3'	5'-GCCCGTAGTGCTTCAGCTT-3'
Ppib #2	5'-GCATACGGGTCCTGGCATCTTGT-3'	5'-ATGGTGATCTTCTTGCTGGTCTT-3'
Nd1	5'-GTTGGTCCATACGGCATTTT-3'	5'-TGGGTGTGGTATTGGTAGGG-3'
Nd2	5'-GCCTGGAATTCAGCCTACTAGC-3'	5'-GGCTGTTGCTTGTGTGACGA-3'
Nd4	5'-CGCCTACTCCTCAGTTAGCCA-3'	5'-TGATGTGAGGCCATGTGCGA-3'
Cytb	5'-CCTTCATGTCGGACGAGGCTT-3'	5'-TGCTGTGGCTATGACTGCGAA-3'
Cox1	5'-TAGCCCATGCAGGAGCATCA-3'	5'-TGGCTGGGGGTTTCATGTTGA-3'
Cox2	5'-ACCTGGTGAACTACGACTGCT-3'	5'-CCTAGGGAGGGGACTGCTCA-3'
Cox3	5'-CTTCACCATCCTCCAAGCTTCA-3'	5'-AGTCCATGGAATCCAGTAGCCAT-3'
Atp6	5'-TGGCATTAGCAGTCCGGCTT-3'	5'-ATGGTAGCTGTTGGTGGGCT-3'
Atp8	5'-TTCCCACTGGCACCTTCACC-3'	5'-TGTTGGGGTAATGAATGAGGCAA-3'
Ucp1	5'-AAGCTGTGCGATGTCCATGT-3'	5'-AAGCCACAAACCCTTTGAAAA-3'
Cidea	5'-GGTTCAAGGCCGTGTTAAGG-3'	5'-CGTCATCTGTGCAGCATAGG-3'
Pgc1a	5'-AACCACACCCACAGGATCAGA-3'	5'-TCTTCGCTTTATTGCTCCATGA-3'
Prdm16	5'-GCACGGTGAAGCCATTCATATG-3'	5'-TCGGCGTGCATCCGCTTGTG-3'
Dio2	5'-GTCCGCAAATGACCCCTTT-3'	5'-CCCACCCACTCTCTGACTTTC-3'
Cpt1b	5'-GCTGCCGTGGGACATTC-3'	5'-CTTGGCTACTTGGTACGAGTTCTC-3'
Adrb1	5'-GCTGGGAGTACGGCTCCTT-3'	5'-GCCGTCACACACAGCACAT-3'
Adrb3	5'-TCCTTCTACCTTCCCCTCCTT-3'	5'-CGGCTTAGCCACAACGAACAC-3'
Pparg	5'-CAAGAATACCAAAGTGCGATCAA-3'	5'-GAGCTGGGTCTTTTCAGAATAATAAG-3'
Adipoq	5'-CAGTGGATCTGACGACACCAA-3'	5'-GAACAGGAGAGCTTGCAACAGT-3'
Cox8b	5'-GCTGGCTGGACTCTGTCATT-3'	5'-GTACCAGGGCCTGCATAGTG-3'
Pgc1b	5'-GAGGGCTCCGGCACTTC-3'-3'	5'-CGTACTTGCTTTTCCCAGATGA-3'
Ppara	5'-ACAAGGCCTCAGGGTACCA-3'	5'-GCCGAAAGAAGCCCTTACAG-3'
Elovl3	5'-TTCTCACGCGGGTTAAAAATG-3'	5'-GGGCCTTAAGTCCTGAAACGT-3'
Bmp8b	5'-CACTTCCGCCGTGGAGC-3'	5'-GTGGGCTAAGACCCATCCTG-3'
Fabp4	5'-AGTGAAAACTTCGATGATTACATGAA-3'	5'-GCCTGCCACTTTCCTTGTG-3'
Nrf1	5'-TGCTTCAGAACTGCCAACCA-3'	5'-GGTCATTTCACCGCCCTGTA-3'
Irf4	5'-AGCTGCAAGTGTTTGCTCAC-3'	5'-GTCTGGCTAGCAGAGGTTCC-3'
Tfam	5'-CCGAAGTGTTTTTCCAGCAT-3'	5'-GGCTGCAATTTTCCTAACCA-3'
Fgf21	5'-CCTCTAGGTTTCTTTGCCAACAG-3'	5'-AAGCTGCAGGCCTCAGGAT-3'

References

1. Wu J*, et al.* Beige adipocytes are a distinct type of thermogenic fat cell in mouse and human. *Cell* **150**, 366-376 (2012).

2. Harms M, Seale P. Brown and beige fat: development, function and therapeutic potential. *Nat Med* **19**, 1252-1263 (2013).

3. Inagaki T, Sakai J, Kajimura S. Transcriptional and epigenetic control of brown and beige adipose cell fate and function. *Nat Rev Mol Cell Biol* **17**, 480-495 (2016).

4. Feldmann HM, Golozoubova V, Cannon B, Nedergaard J. UCP1 ablation induces obesity and abolishes diet-induced thermogenesis in mice exempt from thermal stress by living at thermoneutrality. *Cell Metab* **9**, 203-209 (2009).

5. Cannon B, Nedergaard J. Metabolic consequences of the presence or absence of the thermogenic capacity of brown adipose tissue in mice (and probably in humans). *Int J Obes (Lond)* **34 Suppl 1**, S7-16 (2010).

6. Qiu Y*, et al.* Eosinophils and type 2 cytokine signaling in macrophages orchestrate development of functional beige fat. *Cell* **157**, 1292-1308 (2014).

7. Ohno H, Shinoda K, Spiegelman BM, Kajimura S. PPARgamma agonists induce a white-to-brown fat conversion through stabilization of PRDM16 protein. *Cell Metab* **15**, 395-404 (2012).

8. Loh YH, Zhang W, Chen X, George J, Ng HH. Jmjd1a and Jmjd2c histone H3 Lys 9 demethylases regulate self-renewal in embryonic stem cells. *Genes Dev* **21**, 2545-2557 (2007).

9. Okada Y, Scott G, Ray MK, Mishina Y, Zhang Y. Histone demethylase JHDM2A is critical for Tnp1 and Prm1 transcription and spermatogenesis. *Nature* **450**, 119-123 (2007).

10. Kuroki S*, et al.* Epigenetic regulation of mouse sex determination by the histone demethylase Jmjd1a. *Science* **341**, 1106-1109 (2013).

11. Yamane K*, et al.* JHDM2A, a JmjC-containing H3K9 demethylase, facilitates transcription activation by androgen receptor. *Cell* **125**, 483-495 (2006).

12. Ohguchi H*, et al.* The KDM3A-KLF2-IRF4 axis maintains myeloma cell survival. *Nat Commun* **7**, 10258. doi: 10.1038/ncomms10258 (2016).

13. Abe Y*, et al.* JMJD1A is a signal-sensing scaffold that regulates acute chromatin dynamics via SWI/SNF association for thermogenesis. *Nat Commun* **6**, 7052. doi: 10.1038/ncomms8052 (2015).

14. Tateishi K, Okada Y, Kallin EM, Zhang Y. Role of Jhdm2a in regulating metabolic gene expression and obesity resistance. *Nature* **458**, 757-761 (2009).

15. Inagaki T*, et al.* Obesity and metabolic syndrome in histone demethylase JHDM2a-deficient mice. *Genes Cells* **14**, 991-1001 (2009).

16. Klose RJ, Zhang Y. Regulation of histone methylation by demethylimination and demethylation. *Nat Rev Mol Cell Biol* **8**, 307-318 (2007).

17. Bintu L*, et al.* Dynamics of epigenetic regulation at the single-cell level. *Science* **351**, 720-724 (2016).

18. Barth TK, Imhof A. Fast signals and slow marks: the dynamics of histone modifications. *Trends Biochem Sci* **35**, 618-626 (2010).

19. Pan D*, et al.* Jmjd3-Mediated H3K27me3 Dynamics Orchestrate Brown Fat Development and Regulate White Fat Plasticity. *Dev Cell* **35**, 568-583 (2015).

20. Sakakibara I*, et al.* Fasting-induced hypothermia and reduced energy production in mice lacking acetyl-CoA synthetase 2. *Cell Metab* **9**, 191-202 (2009).

21. Tanaka T*, et al.* Activation of peroxisome proliferator-activated receptor delta induces fatty acid beta-oxidation in skeletal muscle and attenuates metabolic syndrome. *Proc Natl Acad Sci U S A* **100**, 15924-15929 (2003).

22. Shinoda K*, et al.* Phosphoproteomics Identifies CK2 as a Negative Regulator of Beige Adipocyte Thermogenesis and Energy Expenditure. *Cell Metab* **22**, 997-1008 (2015).

23. Cannon B, Nedergaard J. Nonshivering thermogenesis and its adequate measurement in metabolic studies. *J Exp Biol* **214**, 242-253 (2011).

23. Matsumura Y*, et al.* H3K4/H3K9me3 Bivalent Chromatin Domains Targeted by Lineage-Specific DNA Methylation Pauses Adipocyte Differentiation. *Mol Cell* **60**, 584-596 (2015).

24. Inagaki T*, et al.* The FBXL10/KDM2B scaffolding protein associates with novel polycomb repressive complex-1 to regulate adipogenesis. *J Biol Chem* **290**, 4163-4177 (2015).

25. Hayashi-Takanaka Y*, et al.* Tracking epigenetic histone modifications in single cells using Fab-based live endogenous modification labeling. *Nucleic Acids Res* **39**, 6475-6488 (2011).

26. Manke T, Roider HG, Vingron M. Statistical modeling of transcription factor binding affinities predicts regulatory interactions. *PLoS Comput Biol* **4**, e1000039 (2008).

27. Harms MJ*, et al.* PRDM16 binds MED1 and controls chromatin architecture to determine a brown fat transcriptional program. *Genes Dev* **29**, 298-307 (2015).

28. Turner BM. Cellular memory and the histone code. *Cell* **111**, 285-291 (2002).

29. Kajimura S, Spiegelman BM, Seale P. Brown and Beige Fat: Physiological Roles beyond Heat Generation. *Cell Metab* **22**, 546-559 (2015).

30. Cannon B, Nedergaard J. Nonshivering thermogenesis and its adequate measurement in metabolic studies. *J Exp Biol* **214**, 242-253 (2011).

31. Golozoubova V, Cannon B, Nedergaard J. UCP1 is essential for adaptive adrenergic nonshivering thermogenesis. *Am J Physiol Endocrinol Metab* **291**, E350-357 (2006).

32. Kong X, *et al.* IRF4 is a key thermogenic transcriptional partner of PGC-1alpha. *Cell* **158**, 69-83 (2014).

33. Qiang L, *et al.* Brown remodeling of white adipose tissue by SirT1-dependent deacetylation of Ppargamma. *Cell* **150**, 620-632 (2012).

34. Villanueva CJ, *et al.* Adipose subtype-selective recruitment of TLE3 or Prdm16 by PPARgamma specifies lipid storage versus thermogenic gene programs. *Cell Metab* **17**, 423-435 (2013).

35. Rajakumari S, *et al.* EBF2 determines and maintains brown adipocyte identity. *Cell Metab* **17**, 562-574 (2015).

36. Cohen P, *et al.* Ablation of PRDM16 and beige adipose causes metabolic dysfunction and a subcutaneous to visceral fat switch. *Cell* **156**, 304-316 (2014).

37. Shinoda K, *et al.* Genetic and functional characterization of clonally derived adult human brown adipocytes. *Nat Med* **21**, 389-394 (2015).

38. Altarejos JY, Montminy M. CREB and the CRTC co-activators: sensors for hormonal and metabolic signals. *Nat Rev Mol Cell Biol* **12**, 141-151 (2011).

＜謝辞＞

本研究を進めるにあたり、終始懇篤なる御指導とご鞭撻を賜りました 東京大学先端科学技術研究センター 代謝医学分野 酒井寿郎 教授に心から感謝を申し上げます。

本研究に着手するきっかけを頂き、さらに御助言と御協力を賜りました 東京大学薬学部衛生化学教室 新井洋由 教授、河野望 准教授に厚く御礼申し上げます。

本研究の遂行のため、懇切丁寧なご指導を賜りました東京大学先端科学技術研究センター 代謝医学分野 稲垣毅 准教授（現：群馬大学生体調節研究所 代謝エピジェネティクス分野教授)、松村欣宏 准教授、阿部陽平 博士（現：UCSD)、高橋宙大 様、システム生物医学分野 児玉 龍彦 教授、田中 十志朗 教授に深謝申し上げます。

マウス耐糖能試験で大変御世話になりました 東京大学医学部付属病院　糖尿病・代謝内科 門脇孝 教授、国際医療研究センター病院 糖尿病研究センター長 植木浩二郎先生に深く感謝申し上げます。

RNA シークエンス解析で大変御世話になりました 東京大学アイソトープ総合センター 和田研究室　田口明糸 先生に深く感謝申し上げます。

ChIP シークエンス解析で大変御世話になりました 東京大学先端科学技術研究センター　ゲノムサイエンス分野　油谷浩 教授に深く感謝申し上げます。

プロテオミクス解析で大変御世話になりました 東京大学アイソトープ総合センター プロテオミクス研究室　川村猛 准教授に深く感謝申し上げます。

Im-scWAT 細胞を提供してくださり、有意義な御討論を頂きました カリフォルニア大学サンフランシスコ校 梶村真吾 教授に深く感謝申し上げます。

組織切片の作製、並びに免疫染色法のご指導を賜りました 新潟医療専門学校
八神淑英 先生に深く感謝申し上げます。

日々の研究において、有意義な討論や御助力を賜りました 東京大学先端科学技術研究センター　代謝医学分野 内田あおい 様、長尾則子 様、小山 一貴 様、大木翔太郎 様

をはじめ、研究室の皆様に心より御礼申し上げます。

最後に、いつも応援し、温かく見守ってくれた、父 宏人、母 机志子、妹 早希世に深く感謝致します。

平成 31 年 3 月 10 日